TÉCNICO LISBOA

Development of hydrogel-nanoparticle systems for wound healing

Inês Vitória Duarte

Thesis to obtain the Master of Science Degree in

Biological Engineering

Supervisor(s): Prof. Pedro Ricardo Martins Lopes da Fonte
Prof. Duarte Miguel De França Teixeira do Prazeres

Examination Committee

Chairperson: Prof.Maria Margarida Fonseca Rodrigues Diogo
Supervisor: Prof. Pedro Ricardo Martins Lopes da Fonte
Member of the Committee: Prof. André Rolim Baby

January 2021

Declaration

I declare that this document is an original work of my own authorship and that it fulfills all the requirements of the Code of Conduct and Good Practices of the University of Lisbon, Portugal.

Inês Vitória Duarte

Preface

The work presented in this thesis was performed at the Institute for Bioengineering and Biosciences (iBB) of Instituto Superior Técnico (Lisbon, Portugal), during the period March-November 2020, under the supervision of of Prof. Pedro Fonte and Prof. Duarte Miguel Prazeres, and advisership by Prof. Ana Macedo. Due to the Covid-19 pandemic, laboratorial work was limited to the months of July, September, October and November 2020.

This work included the participation in the following papers:

- Marante, T., Viegas, C., Duarte, I., Macedo, A. S., Fonte, P. An overview on spray-drying of protein-loaded polymeric nanoparticles for dry powder inhalation, Pharmaceutics, 12(11), 1032 (2020);
- Pichlsberger, M., Macedo, A. S., Mojsilovic, S., Fonte, P., Kreft, M. E., Lang-Olip, I., Application of perinatal derivatives in animal models on skin wound healing, (in preparation).

And included the participation in the following conferences:

- Duarte, I. Development of insulin-loaded nanoparticle-hydrogel delivery systems to accelerate wound healing, *iMed Conference- Fundação AstraZeneca Innovate Competition*, September 2020
- Duarte, I., Macedo, A., Reis, S., Fonte, P. Optimization of insulin-loaded nanoparticle-hydrogel delivery systems to accelerate wound healing, *NanoPT online conference*, 2020

Acknowledgments

The conclusion of this work would not be possible without the contribution of several people, to whom I want to express my gratitude.

Firstly, I would like to thank Professor Pedro Fonte for all the support, availability and advice given throughout this work. This thesis would not be possible without all the help, guidance and motivation provided, the willingness to listen and teach me, as well as the trust put in me. I finish this chapter academically enriched.

To Ana Macedo, I want to leave my profound thank you for all the help in the lab when something did not go as expected, and for the awesome companionship and conversations in these months. Can not find a word that allows me to thank you with due merit.

I also want to thank to Professor Ana Fernandes-Platzgummer for all the help in the cell culture assays.

I want to leave an acknowledgement to all the team at iBB of Instituto Superior Técnico. Everyone without exception was very friendly and willing to help in any way they could, which provided a great work environment. To them my thank you.

To my four-legged companions, Mimi and Tobias, for all the time I procrastinated while you were taking a nap on top of my computer.

My thanks to all my friends for all the great moments spent, it would most certainly be different without you.

To all my loving family, aunts, uncles, cousins and brother-in-law, my thank you for sharing my accomplishments with me. For my four grandparents, wherever they are, I know they are proud. Thanks, for watching over me.

A special thanks to four of the most important people in my life, my father, mother, sister and nephew. To my nephew for just existing and being the cutest little man, your hug surely cures all the evil in the world. To my sister, for all the love, caring, inspiration and support. Especially, for being my confidant for things that people only tell older siblings. You are definitely the greatest gift our parents could give me, I hope you know that. To my parents for their greatest enthusiasm in all I do, for all the support, emotional and financial, for believing in me, and guiding me throughout my personal and academic life. Thank you for teaching me what's truly important in life, I'm deeply grateful. Every accomplishment of mine will always be yours.

Last but not the least, I thank Diogo for coming along this journey with me. Life is easier by your side. Thank you for all the patience, love, support, laughs, tears, and meals shared all these years. These last five years you kept me going. It would not have been worth it or possible without you.

Resumo

As feridas crónicas representam um problema desafiante, já que as atuais terapias são pouco eficazes, com cicatrização prolongada e recorrências frequentes. A insulina é um dos fatores de crescimento mais barato, que estimula e reduz o tempo de cicatrização. Contudo, o severo efeito proteolítico no leito da ferida, requer um sistema de administração (SA) que proteja a insulina da degradação. O objetivo é desenvolver um SA multifuncional de nanopartículas-hidrogel associado com insulina para acelerar cicatrização das feridas.

As nanopartículas de PLGA revestidas com quitosano e associadas com insulina foram produzidas por dulpa-emulsão e incorporadas em hidrogéis obtidos por congelamento-descongelamento. O SA foi otimizado com uma abordagem de quality-by-design. As nanopartículas foram caracterizadas por DLS e SEM, e os hidrogéis por reologia e FTIR. A estrutura da insulina foi avaliada por CD e testes *in vitro* do perfil de libertação, cell scratch e citotoxicidade foram realizados.

As nanopartículas apresentaram aumento do seu tamanho e alteração positiva do ZP, mostrando um revestimento eficaz de quitosano. Imagens de SEM mostraram incorporação das nanopartículas no hidrogel, mantendo as características sem sinais de agregação. Os resultados revelaram que a estrutura da insulina foi preservada após produção do SA. O SA permitiu uma libertação sustentada da insulina de 10% e 25% até 72h, para as nanopartículas revestidas e não revestidas, respetivamente. Os resultados *in vitro* apenas mostraram migração celular melhorada para o meio de cultura com insulina, fechando a lacuna em 36h, comparativamente com 48h para as restantes condições. Todos os hidrogéis foram considerados biocompatíveis.

Palavras-chave: Cicatrização de feridas; Nanopartícula; Hidrogel; Ferida crónica; Insulina; PLGA.

Abstract

Chronic wounds present a challenging problem, since current therapies are not effective, with extended healing time, high recurrence rates and risk of amputations. Insulin is among the cheapest growth factors available, stimulating wound healing and reducing healing time. However, the harsh proteolytic effect in the wound bed requires a delivery system (DS) able to protect insulin from degradation. The aim was to develop an insulin-loaded multifunctional nanoparticle-hydrogel DS to accelerate wound healing.

Insulin-loaded chitosan-coated PLGA nanoparticles were produced by w/o/w double emulsion technique and embedded in hydrogels obtained by freeze-thawing. The DS was optimized by quality-by-design approach. Nanoparticles were characterized by DLS and SEM, and hydrogels by rheology and FTIR. Insulin structure was evaluated by CD, and *in vitro* release profile, cell scratch and citotoxicity tests were performed.

The nanoparticles showed particle size increase and positive ZP change, showing an effective chitosan coating. SEM images showed that nanoparticles incorporated into the hydrogel, maintaining its features without signs of particle aggregation. The results revealed that insulin structure was preserved upon encapsulation and production of the hydrogel. The nanoparticle-hydrogel allowed a sustained insulin release of 10% and 25% up to 72h, for the insulin uncoated and chitosan coated nanoparticles, respectively. *In vitro* cell scratch assay did not show enhanced cell migration for the hydrogel-nanoparticles systems developed, but showed enhanced cell migration for the culture medium with insulin, closing the gap at 36h, versus 48h for the other conditions. The cytotoxicity was evaluated and all hydrogels were considered biocompatible.

Keywords: Wound healing; Nanoparticle; Hydrogel; Chronic wound; Insulin; PLGA.

Contents

List of Figures

List of Tables

List of Abbreviations and Acronyms

AE association efficiency

CD circular dichroism

CW Chronic wounds

DDS drug delivery systems

DMEM Dulbecco's Modified Eagle's Medium

EC endothelial cells

ECM extracellular matrix

EGF epidermal growth factor

EPC endothelial progenitor cells

ERK 1/2 extracellular signal-regulated kinase 1/2

FBS fetal bovine serum

FGF fibroblast growth factor

FTIR fourier-transform infrared spectroscopy

GF growth factors

HPLC high-performance liquid chromatography

IGF insulin-like growth factor

LC loading capacity

MAPK/ERK mitogen activated protein kinase pathway

MCP-1 monocyte chemotactic protein-1

MIP-1a macrophage inflammatory protein-1α

MMP matrix metalloproteinase

MSC Mesenchymal stromal cells

PBS phosphate-buffered saline

PCL poly(ϵ-caprolactone)

PdI polydispersity index

PDGF platelet-derived growth factor

PGA polyglycolic acid

PI3K/Akt phosphatidylinositol-3-kinase pathway

PLA polylactic acid

PLGA poly(lactic-co-glycolic acid)

PLLCL poly(l-lactide-co-ϵ-caprolactone)

PVA poly(vinyl alcohol)

SEM scanning electron microscopy

TGF transforming growth factor

VEGF vascular endothelial growth factor

WH wound healing

Chapter 1

Introduction

The amount of people suffering from Chronic wounds (CW) is a growing worldwide health and economic problem due to the increasing prevalence of obesity, chronic diseases, and in general, high-risk population like elderly people [1–3]. It is believed that 1-2% of the European and United states population are affected by this, and for example, the incidence of diabetic ulcers alone has reached 10-22% of diabetic patients [4], with the number of diabetic people reaching 20 million, and expected to double by 2030, in the USA alone [5]. It is estimated that a single diabetic ulcer comes with a cost of nearly US$50,000 and CW covers as a whole US$25 billion per year. In Europe, the cost related to wound management is 6,000-10,000€ per patient and year [6]. Besides this, the market for wound care is around US$15 billion and for wound scarring another US$12 billion [5].

Since the traditional existing treatments cannot guarantee effective healing, with a long-lasting therapy and with a relapse rate of about 70%, it ends up being a heavy socioeconomic burden for the national healthcare systems and the patients [4]. Besides this, patients are at risk of amputations, posing a bigger hurdle to caregivers and the life quality of the patient [7].

The eager for an effective treatment to improve life quality for these patients, and the astonishing budget spend for wound care, are what significantly drives the research for better wound healing (WH) alternatives [4]. Significant efforts have been made in that regard, with the search for new treatments and the improvement of existing ones by understanding the numerous factors involved in normal and pathological tissue repair [8].

In this chapter a theoretical background is presented, starting with the anatomophysiology of the skin and continuing with the characterization of acute and chronic wounds, and their healing mechanism. An explanation on the current treatments follows, as well as treatment alternatives, portraying the importance and advantages of the use of nanoparticles, bioactive drugs and hydrogels in drug delivery systems (DDS).

1.1 Anatomophysiology of the skin

Skin is the largest and one of the most important organs of the human body as it covers the entire exterior of the body, providing an essential and effective barrier between the body and the environment. This self-renewing and self-repairing interface protects the body against mechanical, chemical, osmotic, UV light and thermal damage as well as microorganisms invasion [4, 7]. Besides protection, the skin has other functions: sensation - through the different receptors that sense pain, temperature, pressure and touch stimuli; thermoregulation – with the assistance of hair and sweat glands in regulating body temperature, homeostasis is maintained; Metabolism - adipose tissue in the hypodermis is vital in the production of Vitamin D and lipid storage [9]. Healthy skin surface has an acidic pH, between 4.0 and 6.0 and it has a pH gradient reaching approximately pH 7 within the living layers of the epidermis. This pH gradient controls physiological and infectious flora [10]. The skin contains a complex network of nerves to provide sensation, and blood vessels to help maintain thermoregulation and provide nutrients, all distributed in tree layers: epidermis, the external layer, dermis, the middle layer, and hypodermis, the internal layer [8]. The skin layers are shown in Figure 1.1.

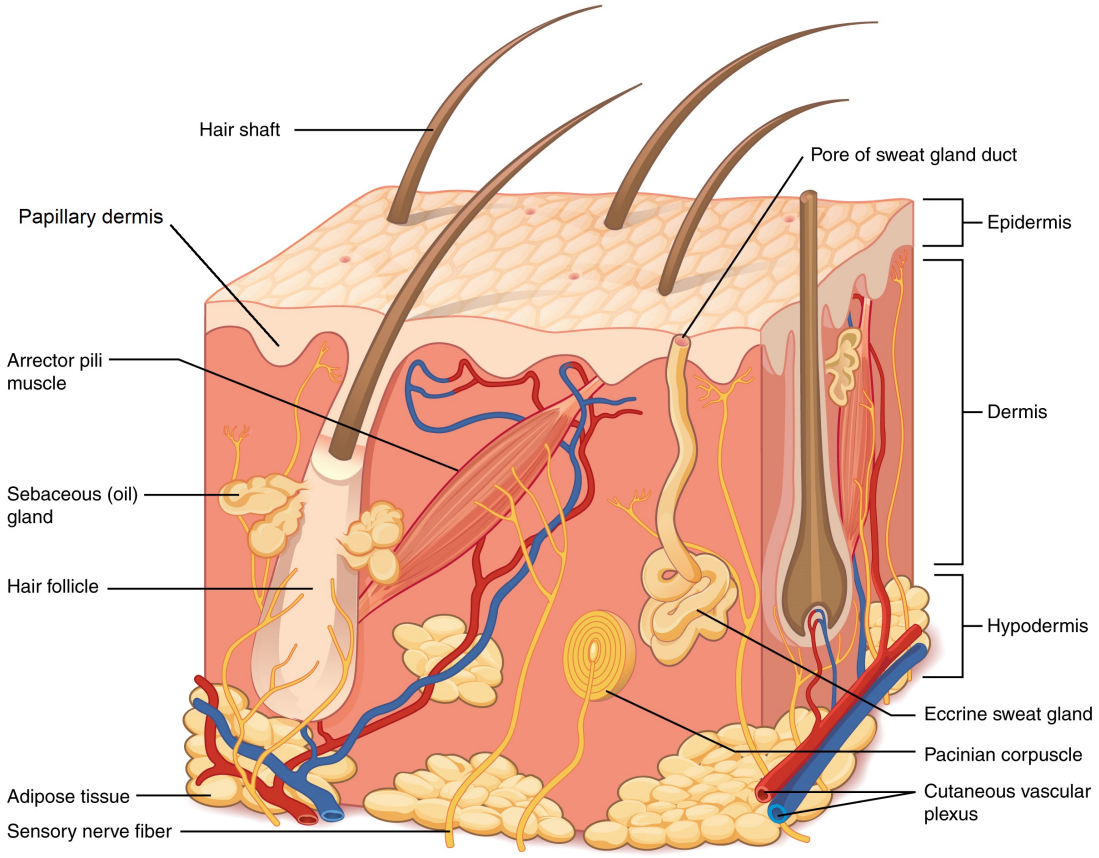

Figure 1.1: Anatomy and organization of human skin. Adapted with permission from [11].

The external layer of the skin, called epidermis, is in the first defence line against exogenous factors, helping maintain homeostasis of the body [9, 10]. The epidermis is composed of epithelial cells, comprising four to five layers depending on its location. From the most external to the most internal layer: *stratum corneum*, *stratum lucidum* (for thick skin only), *stratum granulosum*, *stratum spinosum*

and *stratum basale*. The epidermis layers of the skin are shown in Figure 1.2.

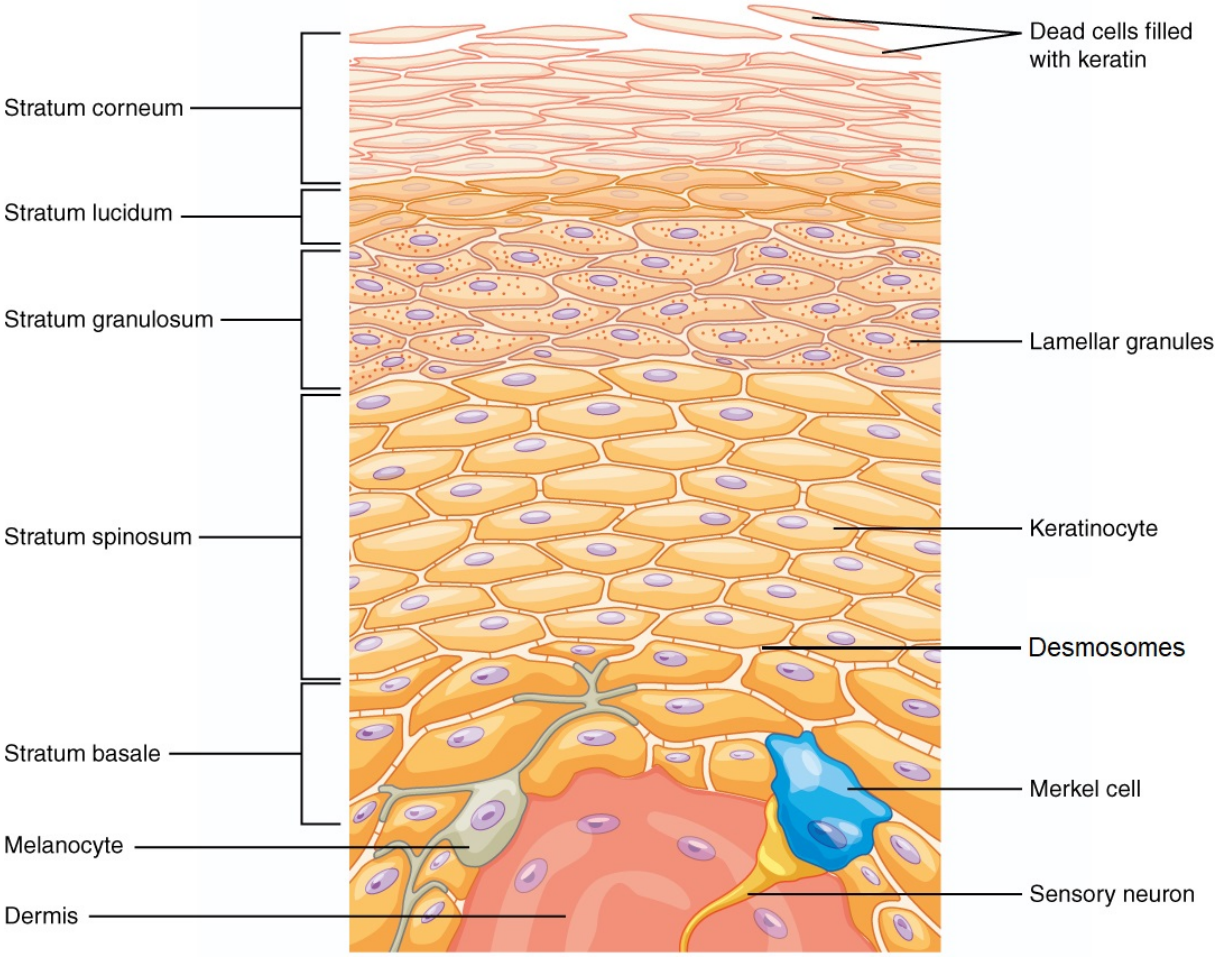

Figure 1.2: Layers of the epidermis (thick skin). Adapted with permission from [11].

The outermost layer is called *stratum corneum*, and it consists of layers of fully cornified dead keratinocytes -corneocytes- and an intercellular matrix rich in fat [12]. This fat-rich composition regulates water loss by preventing fluid evaporation [9] and the dead keratinocytes in this layer secrete defensins, the skin first immune defence [13]. Keratinocytes are the primarily type of cell found in the skin and they express keratin, the main protein in the skin that confers rigidity and helps form the skin barrier protection. In the innermost part of this layer, cells are close to each other, but as it gets near to the exterior, the cells start getting looser and scaling, a process called desquamation [10].

The next layer only exists in the thick skin of soles and palms, it is called *stratum lucidum* and consists of a majority of immortalized cells. The *stratum granulosum* (granular cell layer) follows, and it comprises many layers of cells with lipid-rich granules. These lamellar granules contain glycolipids secreted to the surface of the cells, acting as the glue, keeping the cells together [13]. In this level, as cells are further away from the nutrients present in the deeper tissues, they start to immortalize [9].

The subsequent layer, called *stratum spinosum*, (prickle cell layer) is composed of numerous cell layers connected by desmosomes. Desmosomes are adhesive protein complexes localized in the intercellular junctions, allowing a tightly bound and a contact point between cells, as well as maintaining the mechanical integrity of the tissues. This layer represents most of the epidermis [9].

The layer deepest and closest to the dermis is the *stratum basale* (Basal cell layer). It is separated from the dermis by the basement membrane and it contains stem cells, melanocytes and a single row of keratinocytes, all bound with desmosomes, just like in the *stratum spinosum* layer. Melanocytes are melanin-producing cells, the substance responsible for skin colour, and also protect against ultraviolet radiation damage [11]. The stem cells from this layer are mitotically active, which means they are constantly producing keratinocytes, that in turn, travel outward/upward, evolving and maturating to create the other layers [9, 13]. The merkel cells are also present in this layer, above the basement membrane, and they act as sensory mechanoreceptors for light touch, interacting with free nerve endings in the skin, being very populous in the fingertips [13].

Under the epidermis is situated another skin layer: the dermis. Connecting these two layers, at the basement membrane level, there is a formation of tiny finger-like projections that extend into the epidermis called papillary dermis. In the lower layer of the dermis is located the reticular dermis (see Figure 1.3). The papillary and reticular layers merge without clear demarcation. The papillary dermis is thinner and composed of loose connective tissue, and the deeper reticular layer is thicker, with less cellular content, and denser connective tissue and collagen fibres bundles [13]. The dermis provides strength and flexibility to skin, mainly due to the presence of collagen and elastin. In addition, the dermis also contains blood vessels, nerve endings and other structures like sweat and sebaceous glands [9].

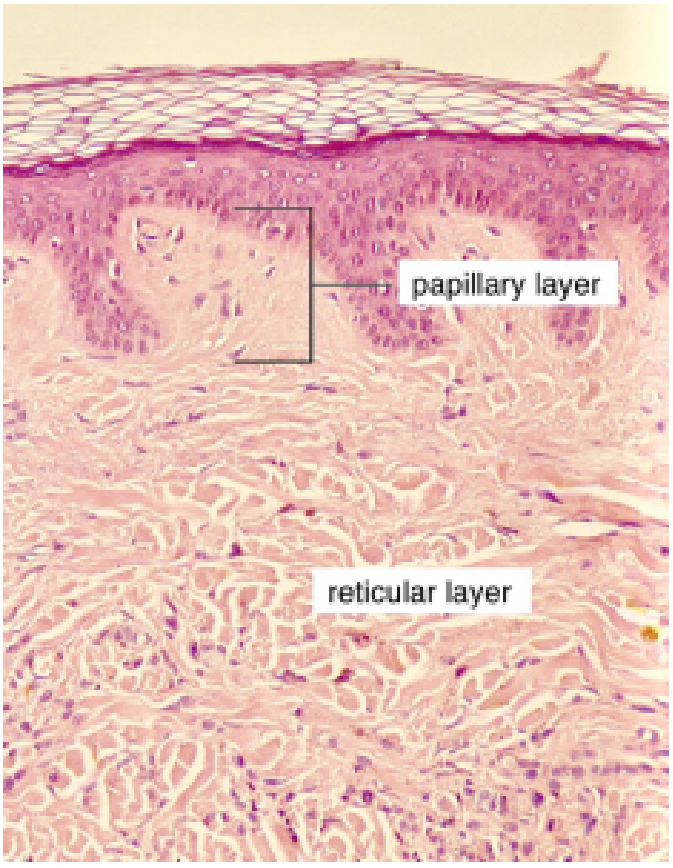

Figure 1.3: Layers of the Dermis: the papillary and the reticular layer. Reprinted with permission from [11].

There are two types of sweat glands, eccrine and apocrine. Eccrine sweat glands are simple, coiled

and tubular glands existing throughout the body, serving as thermoregulatory agents by releasing water to the skin surface, where it evaporates, cooling the skin and blood, and can also participate in ion and nitrogenous waste excretion. Apocrine sweat glands are known for producing malodorous perspiration and are confined to the axillary and perineal regions. They excrete a protein-rich product, initially odorless, but may evolve odor after exposure to bacteria. Modified apocrine sweat glands can include wax-producing ceruminous glands, in the external auditory meatus, moll glands, in the margins of the eyelids and the mammary glands of the breast [14].

Sebaceous glands provide 90% of the skin surface lipids, as the production of sebum is their most important function for maintaining skin homeostasis, lubrication and physiological defense against environmental and infectious attacks. Besides sealing the moisture of the skin and preventing desiccation, sebum also contains antimicrobial substances, free fatty acids and matrix metalloproteinase (MMP) protecting the skin from external insults. Sebocytes, the sebaceous gland cells, engage in lipid synthesis and metabolism and possess numerous hormone receptors, making this gland a endocrine organ and a hormonal target as well [15].

The hypodermis is also called the subcutaneous layer and is the deepest layer of the skin, in which the border between the dermis and hypodermis can be difficult to distinguish [8, 9, 13]. Consisting primarily of adipose and loose connective tissue, the dermis also contains hair follicles, sensory neurons and blood vessels. The loose connective tissue serves the function of connecting the skin to the underlying fibrous tissue of the bones and muscles, and the adipose (fatty) tissue provides insulation and cushioning [11].

1.2 Wound Healing

Since the skin is exposed to the environment, it is vulnerable to several external factors. This exposure can result in wounds, caused by trauma or some medical/physiological conditions. The breakage or disruption of skin, damages the anatomical structure and physiological functions are lost. There are generally two types of wounds: acute and chronic. The former is the result of mechanical damage or exposure to extreme heat, irradiation, electrical shock, or corrosive chemicals and normally heal quickly when given proper care. The latter is typically when a wound does not heal in 8-12 weeks, caused by an underlying medical or physiological condition, which make the healing process difficult and longer due to their high reoccurrence rate (unless the root problems are solved) [4, 7]. The wounds can also be classified according to their depth: superficial wounds (affecting a part of the epidermis); partial-thickness wounds (epidermis and dermal layers are disrupted) and full-thickness wounds (subcutaneous fat and deeper tissue are damaged) [4].

1.2.1 Normal wound healing mechanism

The healing process for acute wounds follows a scheduled pathway composed of four stages: haemostasis, inflammation, proliferation, and remodelling or maturation [4, 8, 16]. A representation of the different

stages of the WH sequence is shown in Figure 1.4.

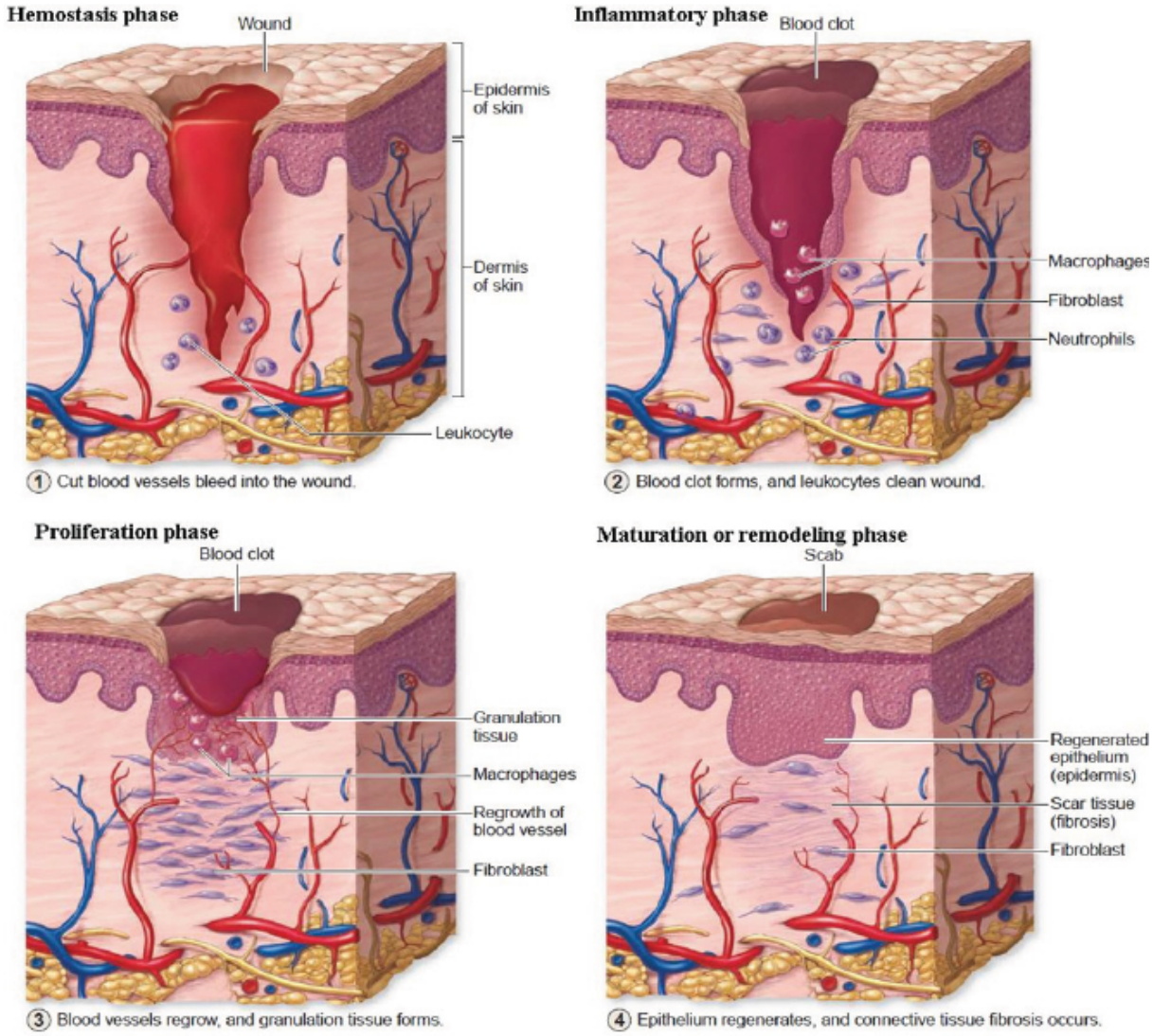

Figure 1.4: Phases of wound healing: hemostasis and inflammation, proliferation, and maturation or remodeling phase. Reprinted with permission from [17].

The WH process begins with the disruption of the epidermal barrier, which immediately prompts haemostasis where the primary goal is to stop the bleeding. Almost immediately vasoconstriction happens as a reflex, as well as blood clotting where platelets form a plug along with fibrin acting as the glue. After drying, this plug is transformed into a scab that serves as a barrier against microorganisms [18]. This scab, during the healing process, also releases cytokines and growth factors (GF), such as epidermal growth factor (EGF), insulin-like growth factor (IGF)-1, platelet-derived growth factor (PDGF), fibroblast growth factor (FGF), transforming growth factor (TGF) (TGF-α and TGF-β) [4], that recruit inflammatory cells, initiating the inflammation [8, 19]. The presence of these GF in the wound bed are very important, because they also attract cells, stimulate their proliferation and have great influence in extracellular matrix deposition, all determinant factors for good wound healing [20].

The inflammation often lasts 2-5 days [4] and its goal is to eliminate any pathogens that may have entered the wound. Since the bleeding has stopped, vasodilation occurs, with an increase in capillary

permeability and influx of phagocytes along with pathogen control. Through the presence of antigenic determinants from invading microorganisms and chemotactic signals from resident cells, the immunological response is activated, and neutrophils, monocytes, leukocytes and macrophages are attracted to the wound site, where GF are further released [4]. Neutrophils are the first to arrive at the site to degrade microbes and dead tissue by phagocytosis. They are also involved in the resolution of the fibrin clot, angiogenesis, and re-epithelialization. Then, chemokines such as monocyte chemotactic protein-1 (MCP-1), macrophage inflammatory protein-1α (MIP-1a) and TGF-β recruit the circulating monocytes that are then differentiated into macrophages. At the beginning of the inflammatory phase, both M1 (with proinflammatory phenotype) and M2 (with anti-inflammatory phenotype) macrophages are found in the wound site, although M2 prevail later in the healing process. By 3-5 days, macrophages are predominant in the wound bed to phagocyte bacteria and necrotic cellular debris, and to release proteases [19, 21].

The influx and activation of inflammatory cells are vital for the transition between inflammatory and proliferative phases. The inflammatory and growth-promoting cytokines, chemokines, GF and nitric oxide secreted by neutrophils and macrophages play a major role in the activation, proliferation and migration of fibroblasts and endothelial cells (EC) from the adjacent dermis, triggering the proliferative phase [8, 19].

The proliferation phase happens generally 3 days to 2 weeks after the trauma and consists of the repair of both epidermal and dermal layers [4, 18]. The increased neovascularization, granulation tissue formation, collagen deposition, and epithelialization are phenomena that occur in this stage. It also consists of the migration and hyper-proliferation of keratinocytes at the wound edge and attraction of fibroblasts, epithelial cells, EC, and circulating and local progenitor cells to start the proliferation process. To re-establish the nutrient and oxygen supply to the wound, neovascularization takes place. The neovascularization process occurs when MMP are released by EC that consequently digest the basement membrane of blood vessels and extracellular matrix (ECM) components. Thus, EC enter the wound bed, proliferating and originating new capillaries. Besides this, bone marrow derived endothelial progenitor cells (EPC) move to the peripheral circulation and later to the wound site where they turn into mature EC, giving rise to new vascular networks and new ECM. This process is regulated by the vascular endothelial growth factor (VEGF) released in a hypoxia condition, that in turn upregulates the production of nitric oxide in the bone marrow, stimulating EPC mobilization and proliferation [22]. Simultaneously with angiogenesis, TGF-b and PDGF from inflammatory cells, mobilize fibroblasts into the area. With the accumulation and proliferation of fibroblasts, new ECM composed of collagen, proteoglycans, and elastin is produced. Some fibroblasts differentiate into myofibroblasts to help with the contraction of the wound and along with keratinocytes, re-epithelialization occurs along the borders of the wound creating a constructive force and eventually closing the wound [19].

In the last phase, remodelling/maturation, varying from 3 weeks to 2 years post-injury, the granulation tissue differentiates giving place to collagen and elastin fibres saturated with proteoglycans and glycoproteins [4]. The blood vessels and cells used for wound repair, and now unneeded, are removed by apoptosis or programmed cell death. The collagen fibers laid down during the proliferative phase, in a disorganized manner, making the wound thick, are now rearranged and replaced by a more orga-

nized matrix structure. The collagen fibers lie closer together and are aligned along tension lines, which reduces scar thickness and gives more tensile strength. Although this coordinated balance between organized matrix production and degradation continues, healed areas are always weaker than uninjured skin, with the tensile strength reaching a maximum of 70 % of that of unwounded skin [4, 5, 8, 23].

1.2.2 Chronic wound healing mechanism

CW are characterized as skin lesions that do not heal within 8-12 weeks and often reoccur [18]. The complex process described above progresses easily for acute wounds, when it is firmly regulated, relying on a balanced molecular environment with GF and cytokines working as the signalling network for the healing process. Sometimes this balanced molecular environment is non-existing, and not regulated, resulting in non-healing CW [6]. The healing process fails when there is an underlying pathology, like diabetes, tumours, immunodeficiency, venous and arterial insufficiency, and metabolic and connective tissue disorders, that breaks up or stalls the orderly sequence of events mentioned above, creating CW. Such wounds comprise decubitus vascular and neuropathic ulcers, several burns, and other chronic ulcerations [18]. A representation of these wounds can be seen in Figure 1.5.

The underlying reasons that cause the disruption of the WH cascade are various. The most common is the continuous inflammatory phase caused by uncontrolled positive feedback. This means that neutrophils are always present in the healing process, and although their target is to kill pathogens preventing the infection of the wound, they can also cause considerable tissue damage to the host by releasing substantial amounts of proteases in the wound bed [26]. This proteolytic microenvironment also causes the degradation of GF, altering the regulation of the process and further delay the healing process. Besides this, in CW, fibroblasts usually present a compromised migration and reduced ability to answer to stimuli, in consequence reducing the formation of new ECM and contraction of the wound in the proliferation phase [6]. Other causes of CW can be impaired macrophages that are ineffective in efferocytosis (competence to phagocyte cells) or neutrophils showing reduced chemotactic and phagocytic activity [27, 28]. The macrophages can also show diminished sensitivity towards biological signals, hence having an altered capability of releasing cytokines, an important element in the healing cascade [29]. Generally, CW have an increased expression and activity of MMP and decreased levels of MMP inhibitors, abnormal neovascularization and nitric oxide levels. Ischemia and vascular diseases (caused by the impaired expression of VEGF and PDGF) also reduce the healing capacity of the wound by restricting leukocytes chemotaxis which leads to impaired pathogen elimination and migration of keratinocytes, fibroblasts and EPC, responsible for tissue regeneration [23, 30]. Moreover, CW, by their long healing periods, are very susceptible to infection, which understandably postpones the healing process [6]. A schematic figure of what happens in a chronic wound healing is represented in Figure 1.6.

In summary, the dysregulated expression and degradation of matrix proteins, GF and cytokines alter the healing process, and traditional wound treatment cannot solve these underlying complications without a special approach [8].

Figure 1.5: Types of chronic wounds: Arterial and venous ulcer, pressure ulcer and diabetic foot ulcer. Adapted with permission from [24, 25].

1.3 Treatment for wound healing

With the increase in chronic wound prevalence, wound care has become very important. The goal of wound management is to prevent infection and accelerate WH with reduced scars and pain for the patient. The applied treatment depends on the wound characteristics, in which phase of the healing process is in, if it is infected, necrotic or with wrong healing, or even if it is exuding or dry [32].

One important existing treatment normally begins with the debridement of the wound. This consists in the removal of dead, damaged, or infected tissue material to expose healthy, well-perfused tissue that is able to proliferate in the wound bed via epithelial cell migration, rather than keeping necrotic tissue that can prompt an infection and stall WH or even cause sepsis. This can either be achieved through mechanical or autolytic/enzymatic mechanisms. Mechanical or surgical debridement timing and frequency are still unclear and depend greatly on the type of wound treated. Despite sometimes causing pain to the patient, it is of general agreement that this procedure is very important and cannot be replaced by autolytic/enzymatic debridement. Autolytic/enzymatic debridement is the self-activation of endogenous

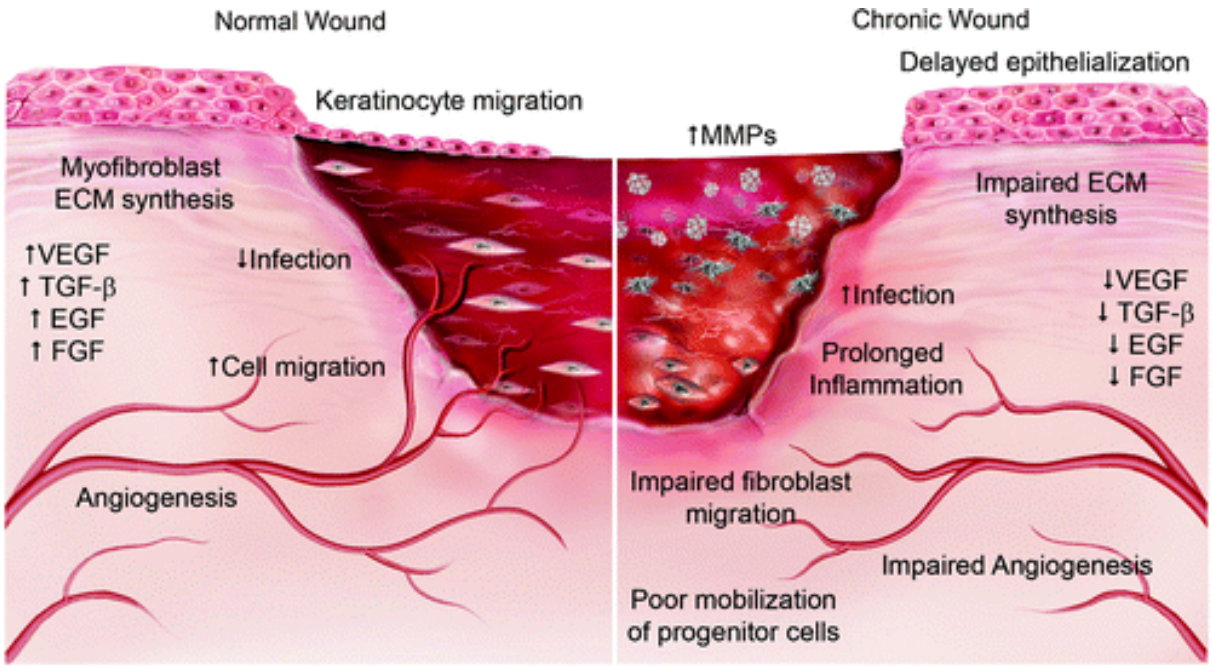

Figure 1.6: Key differences between acute wound and chronic wound healing. Arrows indicate increase (↑) or decrease (↓). Reprinted with permission from [31].

enzymes involved in fibrin degradation generated in a moist wound environment and can be seen in some wound dressings. Lately, there has been some interest in the use of ”biosurgical” debridement, or the application of larvae/maggots to a wound, that interestingly can achieve both mechanical and enzymatic debridement. Although having the capacity of eliminating pathogens and stimulate fibroblast proliferation, it is definitely an intriguing concept but more studies should be performed [5].

Generally, wound care aims to protect the wound from infection and help promote WH. The traditional dry gauze dressing is often not the best option, since it removes the moisture from the wound bed and can cause further injury when removed. A moist occlusive dressing helps in the inflammatory phase because it creates a low oxygen tension environment and increases the rate of re-epithelialization. Besides this, a limited amount of exudate retained in the wound allows for autolytic debridement, which further promotes WH. For these reasons, wound dressing should aim to restrict liquid and microbial penetration, but allow stable moisture and gas exchange environment [5, 33].

When it comes to the prevention of microbial infection, recent developments have focused on integrating antimicrobial compounds in the wound dressing. These antimicrobial compounds could be silver, betaine, chitin, polyhexamethylene biguanide, amoung others. These materials may be appropriate to use in wounds where infection is a problem, especially when there is formation of biofilms, where a barrier is formed, and antibiotics are not able to solve the problem. When this happens, the resolution of the inflammatory phase may be prolonged, and addressing this problem by integrating antimicrobial agents in wound dressing seem to be helpful in chronic pressure/venous ulcers affected by biofilms [34, 35]

Another therapy is the use of autografts and allografts, but the rigorous requirements of donor site limits their usage, and when used, brings along a costly hospital stay. For the allografts, there is even the risk of immune rejection or disease transmission [4]. One of the biggest challenges of traditional

treatment is patient compliance. The existing long-lasting treatments and frequent dressing changes often lead to non-compliance, which is a disadvantage for treatment success [32].

One promising strategy is to administer bioactive endogenous compounds, enhancing their bioavailability, to make up for the absence of them in CW bed [6]. These bioactive molecules are either pro-healing molecules and/or suppressors of elevated protease activity [36]. These molecules, for example, could be GF or other bioactive proteins, essential for their biding to specific receptors to activate the cascade of molecular events for WH [6]. Sadly, due to their protein nature, they are easily degraded by the proteolytic environment in CW, requiring frequent administration. To overcome this problem, the molecules can be incorporated in a DDS, protecting them from protease activity [6]. DDS will be further studied in section 1.4.

A variety of therapeutic agents have been successfully used in patients for various applications. For skin application, in CW specifically, these therapeutic agents could be GF such as insulin, EGF [37] or TGF [38] (among others), hormones [39] and stem cells [8].

In a previous study, human recombinant EGF ointment was used in a rat full thickness wound model, and the results showed significant wound closure from the 5th to the 12th postoperative day compared with the control. This GF increases the rate of epidermal proliferation and accelerates the level of wound contraction related to myofibroblast proliferation and collagen deposition, which all contribute to WH [37]. Another study used PDGF-BB gel in a randomized study with lower extremity diabetic ulcers patients. The study revealed that the administration of PDGF-BB gel in a dose of 100 μg/g in combination of good ulcer care, increased the probability of achieving complete healing by 39% compared with placebo gel [40]. PDGF-BB has been shown to promote formation of granulation tissue at the wound site, and promote wound healing [41]. A different study used VEGF in an ischaemic skin flap rat model, and the results showed higher tensile strength and microvessel density with VEGF treatment when compared with the wounds without treatment. These results suggest that application of VEGF can increase early angiogenesis and tensile strength in ischaemic wounds, something common in chronic wounds [42].

Despite the progressing results, the cost of most GF discourages their application, which is not the case for insulin, one the cheapest GF available.

1.3.1 Insulin as a growth factor

Insulin is an important peptide, hormone and GF, produced by pancreatic b-cells, that regulates blood glucose levels. Besides regulating glucose and lipid metabolism, insulin is involved in processes including protein synthesis, mitochondrial biogenesis, growth, autophagy, proliferation, differentiation, and migration [43]. Insulin has been used to treat diabetes since the early 20th century. As a result of the discovery of recombinant DNA technology, the production of human recombinant insulin was possible and much safer and faster than the old alternative, where porcine and bovine pancreatic tissue was used [44]. This was one the greatest achievements of the 20th century, and opened doors for the worldwide use of insulin for diabetes and other applications like: organ preservation for transplant purposes [45], solution for total parenteral nutrition [46] and WH.

Most cells express insulin receptors - transmembrane glycoprotein - and have a regulated insulin-signalling pathway. Upon insulin binding, autophosphorylation of the insulin receptor occurs, promoting the recruitment of specific adaptor proteins. This leads to the activation of two major downstream signalling pathways: the phosphatidylinositol-3-kinase pathway (PI3K/Akt) and the mitogen activated protein kinase pathway (MAPK/ERK), represented in Figure 1.7.

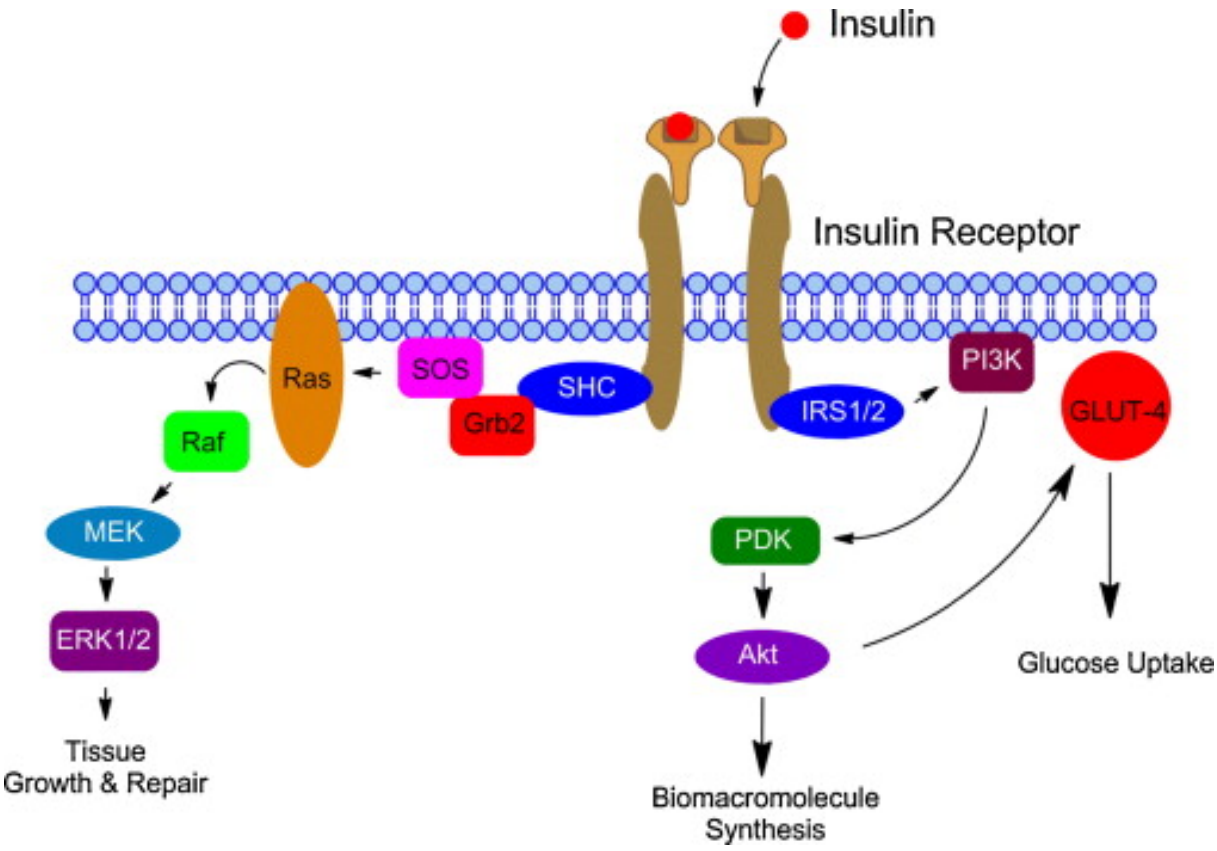

Figure 1.7: Molecular effects of topical insulin in the skin triggering two pathways: PI3K/Akt (right) and MAPK/ERK (left). Reprinted with permission from [47].

The PI3K/Akt pathway activation triggers a cascade of events that regulates the insulin-dependent redistribution of glucose transporter and growth and proliferation responses [48, 49]. The MAPK/ERK pathway consists of MAPK kinase Raf and MEK, and extracellular signal-regulated kinase 1/2 (ERK 1/2). The cascade of events from this pathway also plays a critical role in the mitogenic effects of insulin-like cell proliferation, differentiation, and survival, but is not involved the metabolic regulation like the PI3K/Akt pathway [49, 50]. Additionally, insulin also binds and activates IGF receptors. Generally, insulin regulates several important biological functions in the liver, muscle, adipocytes as well as in the skin [19].

Since the 1930s, insulin has shown to improve WH, when used to treat bedsores in non-diabetic patients [51], and since 1960s when used in diabetic patients with gangrene and decubitus ulcers [16, 52]. Although used in the 60s, few studies have been performed until the late 90s, and recently a growing interest in insulin for WH is showing. The reason for this is because insulin is cheaper, compared to other GF, and approved for human use while having no side effects apart from altering blood glucose levels, which has no effect for topical application at low doses [19]. More recently, some research shows that

topical insulin, insulin solutions, insulin-based sprays, creams and dressings have been successful in the treatment of chronic ulcer in diabetic and non-diabetic patients, and burn wounds in humans and animal models [16].

Insulin was reported to promote growth and development of granulation tissue, accelerate reepithelialisation by stimulating migration and proliferation of keratinocytes, stimulate the migration and tube formation of EC, improving angiogenesis and reducing the healing time [16, 33]. Moreover, [53] showed that with insulin treatment the epidermis assumed a more mature morphology and the blood vessels were more stable.

Concluding, studies suggest that insulin is an effective, safe and strong stimulator of WH in acute or CW. Hence, encapsulating insulin in nanoparticles, protecting them from the peptidase-rich wound environment, and maintaining the bioactivity of insulin could provide all the advantages described above for WH.

1.4 Nanoparticle drug delivery systems

DDS are technologies engineered for the controlled and targeted delivery of therapeutic agents. Developing a new drug is extremely expensive and time-consuming, so, taking advantage of existing "old" drugs and using them with different delivery methods seems to be an attractive choice [54]. DDS control the rate and/or location at which the drug is released and can be used for a variety of applications: anti-tumour therapy, infectious diseases, gene therapy, AIDS therapy, radiotherapy, vaccines, as vesicles to pass the blood-brain barrier, among others. These drugs could be antibiotics, proteins, GF, or even genes [54]. The targeted ability of these systems allows local treatment where increased drug concentrations may be beneficial without exposing the body to high systemic doses of the drug. For topical applications, especially in CW, these systems can improve the patient compliance by delivering an active substance to the wound site and releasing it in a controlled manner for a sustained period of about a week, ultimately solving or minimizing one of the biggest problems of traditional wound treatment [32].

Polypeptides are complex molecules with molecular weights ranging from 5 to 200 kDa, and their stability is very important in peptide-based biopharmaceuticals [55]. GF are one example of these biopharmaceuticals and preserving their amino acid sequence and three-dimensional structure is essential to keep their bioactivity and avoid undesirable immunological reactions [56]. Numerous attempts have been made to provide stability and protection from enzymatic degradation and nanoscale systems have opened new possibilities in this matter. Ideally, a nanomaterial should be easy to design and modify, a natural/biological material, biocompatible, biodegradable, non-cytotoxic and chemically compatible with physiological solutions [8]. These nanoscale systems could be liposomes, polymeric nanoparticles, inorganic nanoparticles, lipid nanoparticles, nanofibrous structures and nanohydrogel (see Figure 1.8) [8, 57, 58].

Nanoparticles are generally defined as "solid colloidal particles with nano-dimension size, about 1-1000 nm" [59]. Compared to microparticles, nanoparticles provide better transport properties and pharmacokinetic profiles, penetrating in deeper tissues due to their small size [8]. Besides this, some

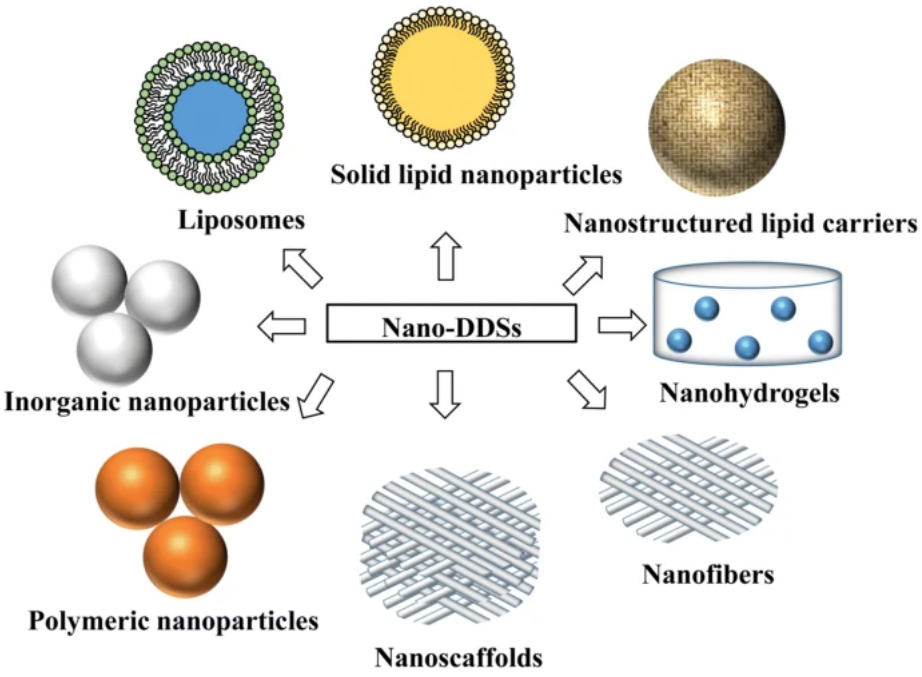

Figure 1.8: Nano scale delivery systems for skin regeneration and wound treatment. Reprinted with permission from [4].

nano DDS are able to enter the cytoplasmic space across cellular barriers or activate specific transport mechanisms [60]. Using nanoparticles can have several other advantages for drug delivery like an increase in drug solubility, prolonged drug release, protect against degradation for bioactive compounds, enhanced bioavailability, and enable a targeted drug delivery while reducing the toxic side effects of the drug [61]. Additionally, for skin application, nanoparticles are also non-toxic and perfectly compatible with the skin, creating a moist environment good for activation and acceleration of the healing process. All these advantages fulfil the checklist for the reduction of dressing change frequency and cost and improvement of patient compliance [4].

1.4.1 Use of polymeric nanoparticles

Natural or synthetic polymers have been extensively used for nanoparticle development. Natural polymers include alginate, gelatine, fibrin, chitosan, collagen, hyaluronic acid, among others. They have great biocompatibility owing to their similarity to macromolecules recognised by the human body. Additionally, some of these polymers have cell biding sites and biomolecular signatures, being involved in the repair of damaged tissue. However, they usually have a high price and can show some batch to batch differentiation, difficulty in controlling the drug release, susceptibility to cross-contamination and presence of immunogenic/pathogenic sections[6]. One study used chitosan nanoparticles loaded with insulin to assess its therapeutic effect in diabetic rats. The results showed that both insulin and empty nanoparticles were able to stimulate inflammatory cell proliferation, angiogenesis and wound maturation. These results could be explained by the fact that the authors could not determine the release of insulin from the nanoparticles. Although using a natural polymer with good wound adhesion, the authors

expect that the high stability of the nanoparticles culminated in a low insulin release [62].

For these reasons, easily controlled and cheaper synthetic polymers could be a reliable alternative. These types of polymers, however, also have a downside, their lake of good cell-recognition sites and poor affinity for cell attachment. Some of the most used synthetic polymers are polylactic acid (PLA), poly(ϵ-caprolactone) (PCL), polyglycolic acid (PGA) and their combination (poly(lactic-co-glycolic acid) (PLGA) and poly(l-lactide-co-ϵ-caprolactone) (PLLCL)) [6]. The use of PLGA nanoparticles loaded with curcumin in a full thickness excisional wound mouse model study showed sustained release up to 76% over a period of 8 days, with consequence of complete wound closure at day 10, compared with 75% of wound closure for the control groups- free curcumin and empty nanoparticles [63].

Some DDS combine these two types of polymers, natural and synthetic, in order to take advantage of the strengths of all components [6].

PLGA

PLGA is a biodegradable, biocompatible hydrophilic and permeable polymer [32, 64] that has been used for peptide delivery vehicles as oral or injectable, but also explored for topical application in WH [64]. PLGA is a polymer approved by FDA and EMA and when hydrolysed generates two monomers, lactic acid and glycolic acid, both metabolized by the body (Figure 1.9). The degradation rate of PLGA can be tailored by varying the relative amount of lactic acid and glycolic acid in the final polymer chain [18].

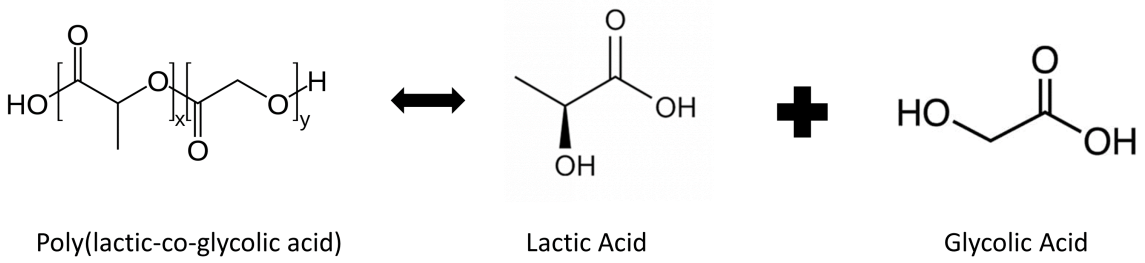

Figure 1.9: Formation of monomers from biodegradability of PLGA.

Chitosan

Chitosan is a positively charged biocompatible and biodegradable polymer (structure in Figure 1.10). Chitosan is also considered to be antimicrobial and has mucoadhesive properties [65, 66]. Besides this, chitosan is known to promote new tissue regeneration through angiogenesis [18], and in general promote WH at different healing stages by alleviating excessive inflammation and infections [65].

1.4.2 Hydrogel as a delivery system

In order to ensure better adherence of the nanoparticles, a substrate is often needed for skin application like gels, foams, membranes or hydrogels. A hydrogel is a soft material with high water content and is

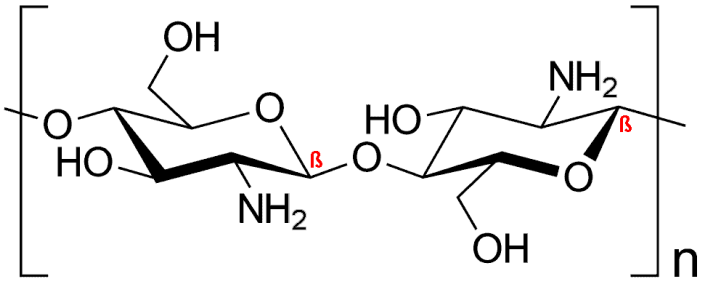

Figure 1.10: Chitosan structure.

usually made of 3-dimensional hydrophilic polymer networks. They can be crosslinked chemically by covalent bonds between polymer chains, or physically by non-covalent interactions such as van der Waals interactions, hydrophobic association, electrostatic interactions or by a combination of both physical and chemical connection. Natural and synthetic polymers are materials used for hydrogel production. Hydrogels have certain characteristics that make them suitable for tissue engineering and drug carriers like their flexibility, water-absorbing and water-retaining properties, biocompatibility and biodegradability. The hydrogel can be administered and match the shape of the damaged tissue, and some can even transform into a gel by responding to environmental stimuli [66]. Using computer programs to create a design to optimize the mechanical functions of the hydrogels is something that has been used for the various tissue engineering applications [67, 68]. Hydrogel can even serve as a wound dressing by creating a moist and occlusive barrier to protect the wound from infection and dehydration while promoting WH [69–71]. Additionally, hydrogels have shown great exudate capacity and avoid secondary damage when changing dressings [66, 72].

Hydrogel synthesized from poly(vinyl alcohol) (PVA), chitosan and silver nanoparticles was used in a study to assess its antibacterial activity and healing rate in a mice model. Results showed that the antibacterial effects were satisfied, and *in vivo* results demonstrate that the groups treated with hydrogel-nanoparticle system showed better wound reduction, especially the hydrogel with 30 ppm silver nanoparticles concentration, compared to control groups [73].

Alginate

Alginate is a low-cost, linear, unbranched polysaccharide obtained from brown seaweed. It is composed of D-mannuronic acid and L-guluronic acid units (Figure 1.11) and its biocompatible, biodegradable, nontoxic and nonimmunogenic [74]. The polyanionic nature of alginate and its structure makes it suitable for highly hydrated hydrogels, where the water is entrapped in the polymer network. Wound dressings using alginate are able to absorb excess wound fluid and maintain a physiological moist environment while minimizing bacterial infections [18, 75].

PVA

PVA is a water-soluble, biocompatible material (structure in Figure 1.12). PVA is used in biomedical applications, in particular, to form gels through freeze-thawing cycles. Despite being non-biodegradable,

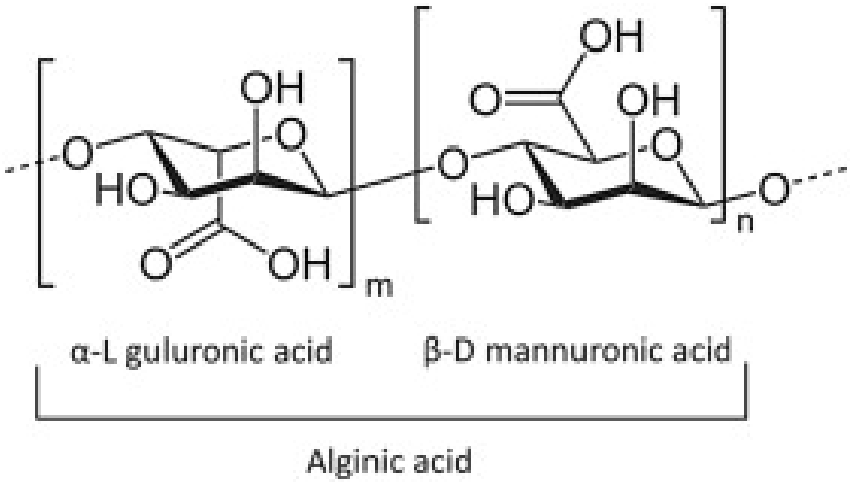

Figure 1.11: Alginate structure and its D-mannuronic acid and L-guluronic acid units.

PVA is easily cleared from the blood via the reticuloendothelial system [59]. The major properties of PVA include crystallizability, adhesion, mechanical strength, and diffusivity. The ease of crosslinking PVA make it a good candidate for the formulations of hydrogels [76, 77].

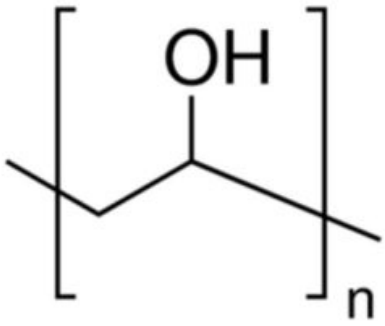

Figure 1.12: Polyvinyl alcohol structure.

Glycerin

Glycerin is a colourless, water-soluble, odourless and viscous liquid with a high boiling point (structure in Figure 1.13). Glycerin has over 1500 known uses for a broad diversity of applications due to its physical or chemical properties. Its non-toxicity and safety have been established through years of safe use, and glycerin is easily metabolized by the body. In the pharmaceutical area its widely used as a solvent, moistener, emollient, humectant and bodying agent in various formulations [78].

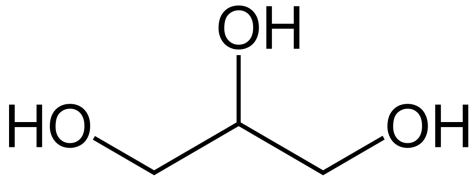

Figure 1.13: Glycerin structure.

Chapter 2

Objectives of the dissertation

The main aim of this work is to develop a nanotechnological multifunctional product for WH. This multifunctional product is a hydrogel embedding insulin-loaded chitosan-coated PLGA nanoparticles. The insulin is used as a GF to promote wound healing. The PLGA is used as the matrix for the nanoparticles, as well as for its prolonged release properties, drug protection and hydrolization of lactic acid. Chitosan is used to coat the nanoparticles to compensate the lack of affinity for cell-recognition of the synthetic polymer, PLGA, used for the nanoparticles. Besides this, chitosan is also considered to be antimicrobial and is know for promoting WH and its mucoadhesive properties. PVA is used to form the hydrogel due to its crosslinking abilities through freeze-thawing cycles. Alginate is also used for the composition of the hydrogel mainly because of its ability of absorbing excess fluid from the wound bed, while maintaining a moist environment and for its gelation properties. Finally, glycerin is used as a moistener, emollient, humectant and bodying agent in the hydrogel formulation. This multifunctional product is intended for a wide use of applications, from acute to chronic wounds, and even burn wounds.

The ultimate goal of this delivery system is to accelerate WH and reduce the frequency of dressing changes, improving the life quality of patients and decreasing the economic burden in healthcare systems. In detail, the objectives of this work are the following:

1. Optimization of the nanoparticle-hydrogel formulation using an experimental design approach. The focus is to obtain nanoparticles with low particle size and high insulin loading, and efficiently coat them with chitosan;
2. Obtaining a nanoparticle-hydrogel by freeze-thawing with good rheological properties and stability for topical application;
3. Ensure the stability of nanoparticles upon hydrogel production by freeze-thawing;
4. Ensure the maintenance of insulin structural stability and bioactivity upon formulation;
5. Evaluate the *in vitro* performance of the nanoparticle-hydrogel formulation;

Chapter 3

Materials and Methods

3.1 Materials

For the nanoparticles production, it was used PLGA 50:50 Resomer RG 503 H (Mw 24,000-38,000; Tg 44-48°C) from Evonik Industries AG (Essen, Germany), chitosan (low molecular weight 50,000-190,000) and recombinant human insulin from Sigma-Aldrich (St. Louis, EUA), dichloromethane from Thermo Fisher Scientific (Waltham, EUA), hydrochloric acid 1M and Acetic Acid glacial from Panreac (Barcelona, Spain).

For the hydrogel production it was used PVA (Mw 89,000-98,000) from Sigma-Aldrich, pharmaceutical glycerine from Ceamed (Funchal, Portugal) and sodium alginate from VWR International, LLC (Radnor, EUA).

For the insulin structure characterization it was used thioflavin T from Acros organics (Geel, Belgium) and chloroform from Thermo Fisher Scientific (Waltham, EUA).

For the high-performance liquid chromatography (HPLC) quantification trifluoroacetic acid and acetonitrile from Thermo Fisher Scientific (Waltham, EUA) were used.

For the *in vitro* assays the used materials were phosphate-buffered saline (PBS) from Sigma-Aldrich, low-glucose Dulbecco's Modified Eagle's Medium (DMEM) and trypsin from Thermo fischer Scientific, fetal bovine serum (FBS) and antibiotic-antimycotic from Gibco (Waltham, EUA).

Different reagents were used to prepare the different solutions, and milli-Q water, produced in-house, used as the solvent for all solutions.

3.2 Preparation of insulin-loaded chitosan-coated PLGA nanoparticles

PLGA nanoparticles were produced using a solvent emulsification-evaporation method based on a water-in-oil-in-water (w/o/w) double emulsion technique, previously developed by our group [79]. Briefly, 200mg of PLGA was dissolved in 2mL of dichloromethane. Then, 0.2 mL of an insulin solution with

150mg/ml in HCL 0.1M was added to the polymer solution. The mixture was sonicated for 45 s with 50% amplitude using a Bandelin sonopuls sonicator from Labometer - Sociedade Técnica De Equipamento De Laboratório Lda (Lisbon, Portugal). After sonication, the primary emulsion was poured to 8mL of PVA 2% (w/v) and further sonicated with the same conditions. The final emulsion was added to another 15mL of PVA 2% (w/v) solution and the organic solvent was completely evaporated in constant magnetic stirring using a RT 15 magnetic stirrer from IKA Werke (Staufen, Germany) for 3 hours.

For the nanoparticles with chitosan coating, a 1.5% (w/v) chitosan in 1% acetic acid (v/v) solution was prepared. This was added to the nanoparticles solution in different amounts, according to the intended chitosan composition of 0.25, 0.5 and 0.75% and let to coat for 4 h. The coated nanoparticles were then washed by centrifugation for 20min at 11000 rpm using a Centrifuge 5810 R from Eppendorf International (Hamburg, Germany) and redipersed in 20mL of PVA 2% (w/v). As controls, unloaded nanoparticles both coated and uncoated with chitosan were prepared.

3.3 Optimization of the nanoparticles-hydrogel formulation

After the nanoparticles production, they were embedded into a polymer solution for gelification by freeze-thawing. Thus, sodium alginate and glycerin were added to the nanoparticle suspension according to the desired composition, and dissolved in constant magnetic stirring for about 3-4 hours. Then, the formulations were subjected to freeze-thawing cycles, in rounds of 6 hours to freeze and 6 hours to thaw at room temperature, using a freezer at -20°C from Liebherr Group (Bulle, Switzerland). The optimization of the hydrogel composition was achieved following a quality by design approach using the Statistica software version 10 by TIBCO Software (Palo Alto, USA). The independent variables were the composition of chitosan (0.25, 0.5 and 0.75%), sodium alginate (1, 1.5 and 2%) and glycerin (5, 7.5 and 10%) and the number of freeze-thawing cycles (1, 2 and 3). The effect of these parameters on the product properties was analysed by evaluating the mean particle size and zeta potential, as well as viscosity and spreadability of the hydrogel (dependent variables). The model chosen was a 2**(k-p) standard design with 4 factors (k=4) (independent variables), 1 block (p=1), 8 runs with a triplicate central point and 4 blank columns for the dependent variables. Using the software it was created the matrix with the hydrogel composition for each experiment, and the Design-Expert program, version 6.0.4 by Stat-Ease Inc (Minneapolis, USA), was also used to obtain the optimal hydrogel formulation based on the different compositions.

3.4 Nanoparticle-hydrogel Characterization

3.4.1 Insulin association efficiency and loading capacity

The amount of insulin carried by the nanoparticles is evaluated by calculating the insulin association efficiency (AE). This calculates the difference between the total amount of insulin used and the amount of free insulin present in the the supernatant after centrifugation, the non-associated insulin. The loading

capacity (LC) is calculated as the ratio in percentage between the amount of insulin associated to the nanoparticles and its total weight. The amount of free insulin is assessed by HPLC (see section 3.4.6) using the supernatant of the formulation after centrifugation. The total weight of the nanoparticles is calculated accordingly with the amount of the polymer used to encapsulate insulin. These parameters are calculated to evaluate if the insulin association was efficient, and to have the information of the amount of insulin in the nanoparticles to use in further tests, like the insulin release profile in section 3.6.1. Therefore, the AE and LC of insulin were determined using the equations (3.1) and (3.2), respectively.

$$AE = \frac{Total\ amount\ of\ insulin\ -\ Free\ insulin\ in\ supernatant}{Total\ amount\ of\ insulin} \times 100 \tag{3.1}$$

$$LC = \frac{Total\ amount\ of\ insulin\ -\ Free\ insulin\ in\ supernatant}{Total\ weight\ of\ nanoparticles} \times 100 \tag{3.2}$$

3.4.2 Particle size and zeta potential analysis

The particles hydrodynamic radius and superficial charge were analysed by dynamic light scattering technique and electrophoretic light scattering, for size and zeta potential analysis, respectively, using a Zetasizer Nano series from Malvern Panalytical (Malvern, United Kingdom). The samples were diluted with milli-Q water with an appropriate dilution for the analysis, and all measurements were performed in triplicate. To evaluate the maintenance of the particle size after hydrogel production, the gelification ratio was calculated by dividing the mean particle size after gelification by the mean particle size before gelification (equation 3.3).

$$Gelification\ ratio = \frac{Mean\ particle\ size\ after\ gelification}{Mean\ particle\ size\ before\ gelification} \tag{3.3}$$

3.4.3 Viscosity, spreadability and water content analysis

The rheological properties of the hydrogel were assessed by evaluating its viscosity, spreadability and water content. These parameters were evaluated to asses the viability of the hydrogel for topical application.

The viscosity was assessed using a DV-II+Pro Viscometer from AMETEK Brookfield (Middleborough, United States) with the CPE-52 spindle and using a 500 μL sample of the hydrogels until 100%, or close, was reached for torque value.

For the spreadability the methodology described by Knorst 1991 [80] was used, with a modification in the sample application mode. The method uses a glass plate with the centre marked, on top of millimetric paper, in which the samples with the same volume (500 μL) were dropped. Predetermined weights of 48.6g, 251.8g and 778g, were put on top of another glass plate, with 1-minute interval. The diameter in opposite directions was measured for all weights, and used to calculated the mean diameter of the hydrogel spread. Three weights were used, and the spreadability (Ei) for each weight was calculated using the following equation:

$$Ei = d^2 \frac{\pi}{4} \tag{3.4}$$

Where d is the mean diameter calculated.

For the water content analysis, weighed samples, of around 1g of hydrogel, were placed in glass vials, previously weighed, and then placed in a Heidolph Instruments (Schwabach, Germany) inkubator 1000 at 66°C for 22 hours. The samples were weighed at 1-hour intervals until a constant weight was reached. The water content was calculated using the following equation:

$$Water\ content\ (\%) = \frac{Hydrogel\ initial\ weight\ -\ Hydrogel\ final\ weight}{Hydrogel\ initial\ weight} \tag{3.5}$$

3.4.4 Scanning electron microscopy

Characterization of the PLGA nanoparticles surface morphology was assessed by scanning electron microscopy (SEM) using an Analytical FEG-SEM: JEOL 7001F microscope from Jeol Ltd. (Tokyo, Japan). The nanoparticles were assessed after production and after the gelification process incorporated in the hydrogel and without the hydrogel. For the nanoparticles after production the samples were prepared by centrifugation at 13,300 rpm for 30 minutes, removing the supernatant and resuspending in the same volume of milli-Q water. For the nanoparticles after gelification without the hydrogel, the hydrogel was diluted by 5x with milli-Q water and centrifugated at 13,300 rpm for 30 minutes, removing the supernatant with hydrogel debris and re resuspending in milli-Q water. Then, the samples were mounted onto metal stubs and vacuum-coated with a layer of gold/palladium before observation in the SEM microscope.

3.4.5 Fourier Transform Infrared Spectroscopy

The fourier-transform infrared spectroscopy (FTIR) spectra were collected using a Nicolet 5700 FT-IR Spectrometer from Thermo Fisher Scientific (Waltham,EUA) with a Smart iTR accessory.

The FTIR spectra were obtained by collection of 256 scans with 4cm^{-1} resolution in the 4000-600 cm^{-1} region. The samples used were the lyophilized hydrogel to minimize the water spectra noise in the FTIR spectra. All samples were run in triplicate and the average is presented.

3.4.6 Insulin quantification by HPLC-UV

The insulin concentration in the samples collected upon nanoparticle production and in the *in vitro* release study was determined using a previously validated reversed-phase HPLC-UV [81]. The HPLC system used was Hitachi Chromaster from VWR International, LLC (Radnor, EUA). The mobile phase of the chromatographic method consists of acetonitrile: 0.1% (v/v) trifluoroacetic acid (TFA) aqueous solution initially set to a ratio of 30:70 (v/v), which is linearly changed to 40:60 (v/v) over 5 min. From 5 to 10min the ratio is kept constant at 40:60 (v/v). The mobile phase is pumped at a constant flow rate of 1 ml/min, the injection volume is 20 μl and the detection wavelength used is 214 nm. The HPLC method was performed using a Waters Corporation (Milford,USA) XTerra RP 18 Column with 4.6mm of

diameter, 250 mm of length and pore of 5.0μm and a LiChrospher 100 RP-18 5μm particle size guard column from Merck KGaA (Darmstadt, Germany). All experiments were performed in triplicate and at room temperature, and the total area of the peak was used to quantify insulin. The calibration curves were prepared using human insulin standard solutions at concentrations of 1, 3, 6, 12.5, 25, 50 and 100 μg/ml.

3.5 Insulin structural characterization

3.5.1 Insulin extraction

To assess the insulin structure after the nanoparticle and hydrogel production, the insulin from the nanoparticle-hydrogel was extracted. For this, hydrogel samples, previously frozen at -80°C, were lyophilized using the Alpha 1-2 LD plus freeze dryer from Martin Christ Gefriertrocknungsanlagen GmbH (Osterode am Harz, Germany) for 48h at a condenser surface temperature of -52°C. To extract the insulin, the samples were submitted to a chloroform treatment to dissolve PLGA and release the insulin. The treatment included the lyophilized hydrogel, 500 μL of HCl 0.1M, and 1mL of chloroform. The mixture was inverted for about 2 minutes so the two phases would mix, and then centrifuge at 5000 rpm for 5 minutes to separate the phases. The bottom phase (cloroform) was excluded and another 1mL of chloroform was added. This was repeated 10 times, and in the end the aqueous phase containing the HCl and dissolved insulin was recovered and used for the protein structure analysis.

3.5.2 Circular dichroism analysis

The measurements using the extracted protein obtained in section 3.5.1 were collected using an π*-180 circular dichroism (CD) spectrometer from Applied Photophysics (Leatherhead, UK) and Pistar software. The lamp housing was continuously purged with nitrogen at a flow of 8L/min at 25°C. The extracted protein solution was diluted with HCl 0.01M to a required concentration in order to avoid the maximum voltage of the equipment. The control protein spectrum was obtained using a 0.2mg/ml solution of insulin in 0.01M HCl. The CD spectra were collected from an average of 3 scans in the 190-250 nm region, with a step of 0.5 nm and averaging time of 5 s using a 0.1 cm cell. The signal was converted to molar ellipticity using with the following equation:

$$\theta = \frac{CD\ signal \times MRW}{10 \times c \times d} \tag{3.6}$$

Where MRW is the mean residual weight of each insulin residue (116 Da), c is the insulin concentration and d the cell pathlength. The insulin concentration was determined by UV absorption at 280 nm in a NanoDrop ND-1000 Spectrophotometer from Thermo Fisher Scientific (Waltham, EUA) and using a molar extinction coefficient of 5800 $M^{-1}cm^{-1}$.

3.5.3 Fluorescence spectroscopy analysis

The extracted protein solution obtained in section 3.5.1 was also used to obtain the fluorescence emission spectra. The spectra were obtained in a 260-400 nm range with 1nm step, with excitation occurring at 280 nm and emission and excitation slits at 10 nm, an averaging time of 0.1 s with a Varian,Inc (Palo Alto, USA) Cary Eclipse Fluorescence Spectrophotometer. The control protein spectrum was obtained using a 0.2mg/ml solution of insulin in 0.01M HCl, and the reference spectrum was obtained with a 0.01M HCl solution. The reference spectrum was auto subtracted from the samples spectra and normalized based on the signal intensity.

3.5.4 Thioflavin T assay

To assess the existence of insulin fibrillation, an indicator of insulin denaturation, a thioflavin T assay was performed. The extracted protein solution obtained in section 3.5.1 was used to run the thioflavin T experiments in a Varian,Inc (Palo Alto, USA) Cary Eclipse Fluorescence Spectrophotometer. The thioflavin T concentration was 25 μM and insulin was around 11 μM. The samples were excited at 450 nm and the intensity measured at 485 nm with both slit widths at 5 nm, and averaging time of 0.1 s. The reference sample intensity was subtracted to the test sample. The positive control was a 0.2mg/ml insulin solution heated overnight at 60°C and the negative control was a fresh 0.2mg/ml insulin solution in 0.01M HCl.

3.6 *In vitro* studies

3.6.1 *In vitro* Insulin release profile

The insulin-loaded PLGA nanoparticles hydrogel samples were used to evaluate the *in vitro* release profile of insulin. The method used was based in [82]. For this method cell culture inserts from Thermo Fisher Scientific (Waltham,EUA) with 8 μm pore size were used since the polycarbonate membrane allows soluble material to pass into the receiver compartment. The hydrogel, previously weight around 1g, was inserted in the inserts. In order to mimic the environment of a wound, the receiver phase was kept at 10mL of pH 7.4 PBS solution and incubated at 33°C under stirring at 150rpm using a Heidolph Instruments Inkubator 1000 and Titramax 1000. The experiment initiated when the inserts containing the hydrogel were suspended in the aqueous receiver phase. Samples of the solution were taken at predetermined time intervals of 0.5h, 1h, 2h, 4h, 8h, 24h, 48h and 72h and fresh medium at the same temperature was replaced to keep the initial volume of the reservoir constant. The collected samples were centrifuged at 13,300 rpm for 30min prior to determination using HPLC methodology. All samples were run in triplicate.

3.6.2 *In vitro* cell scratch assay

Mesenchymal stromal cells (MSC) were cultured with low-glucose DMEM supplemented with 10% (v/v) FBS (FBS MSC qualified) and 1% (v/v)antibiotic-antimycotic (MSC expansion culture medium) and kept at 37°C, 5% CO_2 in a humidified atmosphere. Upon reaching 90% confluence, cells were detached using 0.05% (v/v) Trypsin and counted using the Trypan Blue exclusion method. Cells were sub-cultured into 24-well tissue culture plates at a seeding density of 3000 cells/cm^2. Cells were grown to 100% confluence and scratched using a 200 μL sterile pipette tip. Cells were washed with PBS to remove dead cells and debris, and cultured with the different treatment conditions: A) insulin-loaded chitosan-coated nanoparticle-hydrogel (Ins-Chi-Np-H); B) insulin-loaded nanoparticle-hydrogel (Ins-Np-H); C) chitosan-coated nanoparticle-hydrogel(Chi-Np-H); D) nanoparticle-hydrogel (Np-H); E) Hydrogel; F) MSC expansion culture medium supplemented with insulin 10^{-7} M (CM with insulin) and G) MSC expansion culture medium (culture medium) (2 wells/condition). The conditions A-E were diluted with MSC expansion culture medium (1:20). Cell migration was observed after 24h, 36h and 48h using an Leica DM IL LED microscope with EC3 camera system and the area of cell migration into the scratch was quantified using ImageJ software.

The empty area across the scratch at 0h (a_0) and at each time interval (a_x) were used to calculate the % of empty area in the scratch using the following equation:

$$Empty\ area\ in\ the\ scratch\ (\%) = \frac{a_x}{a_0} \times 100 \tag{3.7}$$

3.6.3 *In vitro* cytotoxicity assay

The biocompatibility of the hydrogels was demonstrated through a cytotoxicity assay using L929 cell line (mouse fibroblasts) according to ISO10993. The cells were cultured with DMEM supplemented with 10% (v/v) FBS and 1% (v/v) antibiotic-antimycotic (L929 expansion culture medium) and kept at 37°C, 5% CO_2 in a humidified atmosphere. Upon reaching 90% confluence, cells were detached using 0.05% (v/v) Trypsin and counted using the Trypan Blue exclusion method. Cells were sub-cultured into 24-well tissue culture plates at a seeding density of 80,000 cells/cm^2. After 24h, spent culture medium was removed and cells were incubated with the different treatment conditions: A) insulin-loaded chitosan-coated nanoparticle-hydrogel (Ins-Chi-Np-H); B) insulin-loaded nanoparticle-hydrogel (Ins-Np-H); C) chitosan-coated nanoparticle-hydrogel (Chi-Np-H); D) nanoparticle-hydrogel (Np-H); E) Hydrogel; F) L929 expansion culture medium supplemented with insulin 10^{-7} M(CM with insulin); G) expansion culture medium supplemented with 10% (v/v) DMSO (positive control) and H) L929 expansion culture medium (negative control) (3 wells/condition). The conditions A-E were diluted with L929 expansion culture medium (1:2 and 1:20) 48h prior to cell incubation. After 48h, the treatment conditions were removed and cells were incubated with MTT solution (1mg/ mL) for 2 h. After the incubation period, MTT solvent (HCl and IPA – 1:100) was added and the plates were stirred for 10 min. Absorbance was quantified at 570 nm to determine total cell viability.

Chapter 4

Results and Discussion

In this chapter, the results will be presented along with the discussion. Starting with the optimization of the nanoparticle-hydrogel formulation using an experimental design approach, where the focus was to obtain nanoparticles with low particle size and high insulin loading, and efficiently coat them with chitosan, as well as obtaining a nanoparticle-hydrogel by freeze-thawing with good rheological properties and stability for topical application. Then, the stability of nanoparticles upon hydrogel production by freeze-thawing will be ensured along with ensuring the maintenance of insulin structural stability and bioactivity upon formulation. Finally, *in vitro* evaluation of the performance of the nanoparticle-hydrogel formulation will be discussed.

4.1 Nanoparticle-hydrogel optimization

The nanoparticles were composed of PLGA and chitosan and the hydrogel was composed of PVA, alginate and glycerin. Each of these components was used for different reasons. The PLGA was used as the matrix for the nanoparticles, and for its prolonged release properties, drug protection and hydrolization of lactic acid. Chitosan was used to coat the nanoparticles to compensate the lack of affinity for cell-recognition of the synthetic polymer, PLGA, used for the nanoparticles. Besides this, chitosan is also considered to be antimicrobial and is know for promoting WH and its mucoadhesive properties. PVA is used to form the hydrogel due to its crosslinking abilities through freeze-thawing cycles. Alginate is also used for the composition of the hydrogel mainly because of its ability of absorbing excess fluid from the wound bed, while maintaining a moist environment and for its gelation properties. Finally, glycerin is used as a moistener, emollient, humectant and bodying agent in the hydrogel formulation.

The hydrogel composition was optimized using a quality-by-design approach which consisted of varying the concentration of chitosan, alginate and glycerin in the nanoparticle-hydrogel and the number of freeze-thawing cycles. These were the variables chosen because they are the ones that contribute most for the hydrogel properties and the nanoparticles mucoadhesive properties, which is the main focus of this optimization. For the optimization of the hydrogel all nanoparticles were prepared without insulin. The chitosan varied between 0.25% and 0.75%, having a center point of 0.5%. The sodium alginate

and glycerin were between 1-2% and 5-10% with a center point of 1.5% and 7.5%, respectively. These variants were given to Statistica software using the DOE option menu with 2**(K-p) standard design. The program returned a matrix with 11 formulations, 3 being the central point triplicates. The matrix given by the program is the Table 4.1.

Table 4.1: Composition of the different formulations given by experimental design, based on the amount of alginate, glycerin, freeze-thawing cycles and chitosan.

Formulation	Alginate (% w/v)	Glycerin (% v/v)	Freeze-Thawing Cycles	Chitosan (% w/v)
A	1	5	1	0.25
B	1	5	3	0.75
C	1	10	1	0.75
D	1	10	3	0.25
E	1.5	7.5	2	0.5
F	1.5	7.5	2	0.5
G	1.5	7.5	2	0.5
H	2	5	1	0.75
I	2	5	3	0.25
J	2	10	1	0.25
K	2	10	3	0.75

4.1.1 Nanoparticles Characterization

After production of the unloaded nanoparticles according to the matrix given by Statistica with the respective chitosan coating, the mean nanoparticle size, polydispersity index (PdI) and zeta potential were assessed to understand the coating effectiveness and the results are shown in Figure 4.1.

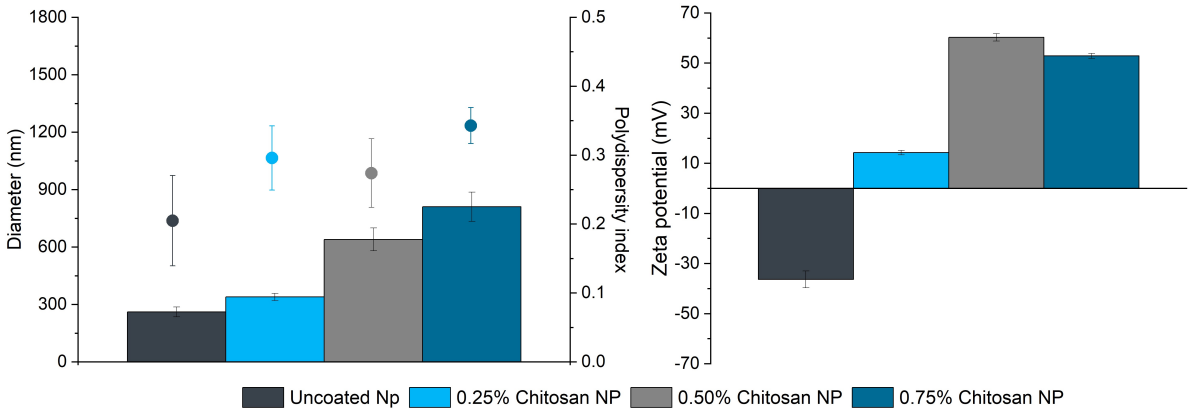

Figure 4.1: Mean particle size (left bars), polydispersity index (interval plot) and zeta potential (right bars) characterization of different concentration chitosan-coated PLGA nanoparticles (n=3, mean ± SD).

The results show an increase in the nanoparticle diameter with the increase in chitosan concentration. In terms of diameter the values were 261.3±26.1 nm, 339.6±18.9 nm, 640.2±59.6 nm and 811.0±76.1 nm for the uncoated nanoparticles, 0.25%, 0.5% and 0.75% chitosan coating, respectively. An increase in the size of the nanoparticles with the increase of chitosan concentration indicates that the

chitosan attached to the nanoparticles, creating a thicker layer around the surface of the nanoparticles, according to what is described in the literature [83].

The zeta potential values were -36.3±3.4 mV, 14.3±0.9 mV, 60.3±1.5 mV and 52.9±1.0 mV for the uncoated nanoparticles, 0.25%, 0.5% and 0.75% chitosan coating, respectively. These values show a change in the coated nanoparticles, exhibiting a positive zeta potential, as opposed to the uncoated nanoparticles that show a negative zeta potential. These results further corroborate the results from the mean particle size, since the change in negative to positive charge can be explained with the fact that chitosan has a positive charge [84].

The results from the diameter and the zeta potential corroborate the effective chitosan coating of the nanoparticles, in fact this coating is more efficient as the chitosan concentration increases.

For the values of PdI they were 0.205±0.03, 0.296±0.02, 0.274±0.02 and 0.343±0.01 for the uncoated nanoparticles, 0.25%, 0.5% and 0.75% chitosan coating, respectively. Since these values revolve around 0.2-0.3, the sample can be considered homogeneous, according to Danaei et al [85].

The gelification of the hydrogel occurs by the addition of alginate and glycerin to the nanoparticle suspension with PVA 2%. The freeze-thawing cycles further gelificate the hydrogel by making crooslinking reactions with water and PVA, causing gelation due to the formation of semi crystalline structures. Based on the mean nanoparticle size, PdI and zeta potential of the nanoparticles after production, it was intended to investigate the effect of the gelification by freeze-thawing cycles in these characteristics.

The mean nanoparticle size and zeta potential after gelification were assessed and the results are shown in Figure 4.2.

The results shown in Figure 4.2 relative to the size of the nanoparticles are variable, which can be due to the gelification process, where particle aggregation might have happened. However the zeta potential values show a difference in the signal comparative to the nanoparticles post production. In post production the nanoparticles were coated with chitosan conferring them a positive charge, but post gelification the nanoparticles were embedded in the hydrogel were the sodium alginate was present, with a negative superficial charge [86]. In this case the negative charge of the sodium alginate camouflaged the chitosan, changing the surface charge of the nanoparticles.

4.1.2 Hydrogel Characterization

With the aim of achieving an optimal formulation with good rheological properties for topical application, it was important to submit the hydrogels to rheological evaluation. Additionally, the macroscopical aspect was taken into account. For the hydrogel characterization the viscosity and spreadability were assessed and photos of the hydrogel after standing still overnight are shown in Figures 4.3 and 4.4, respectively. The different formulations identified from A to K are represented in Table 4.1.

The results from Figure 4.3 show very low viscosity accompanied with high spreadability for formulations A, B, C and D. Furthermore, in Figure 4.4 these formulations showed a deposit in the bottom of the vial, which means that it has less colloidal stability than the other formulations. According to [87, 88] the best viscosity range for topical application is around 1,000-10,000 cP, which further corroborates with

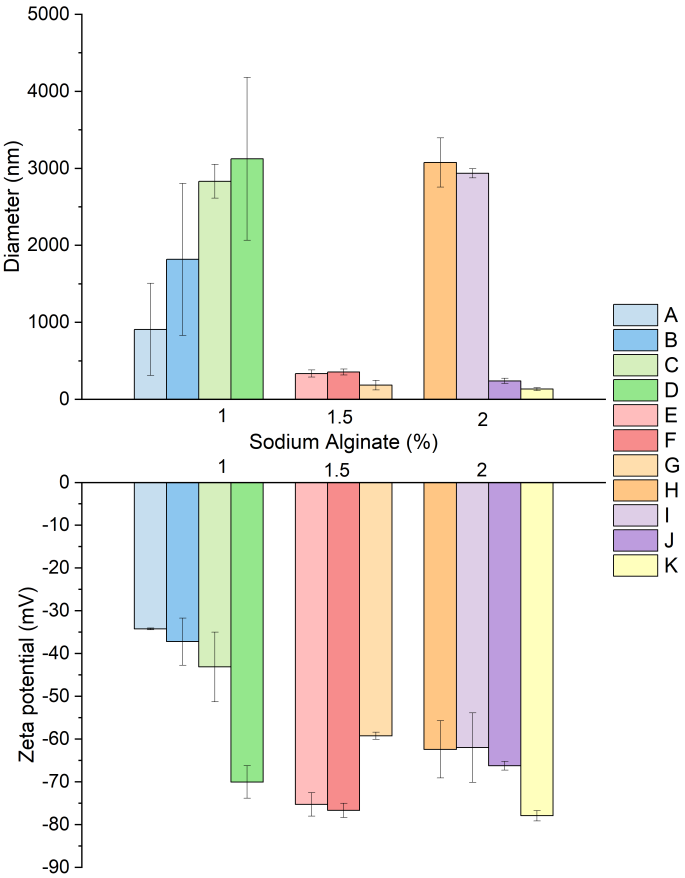

Figure 4.2: Mean particle size (top bars) and zeta potential (bottom bars) characterization of the different composition hydrogels (n=3, mean $\pm$ SD).

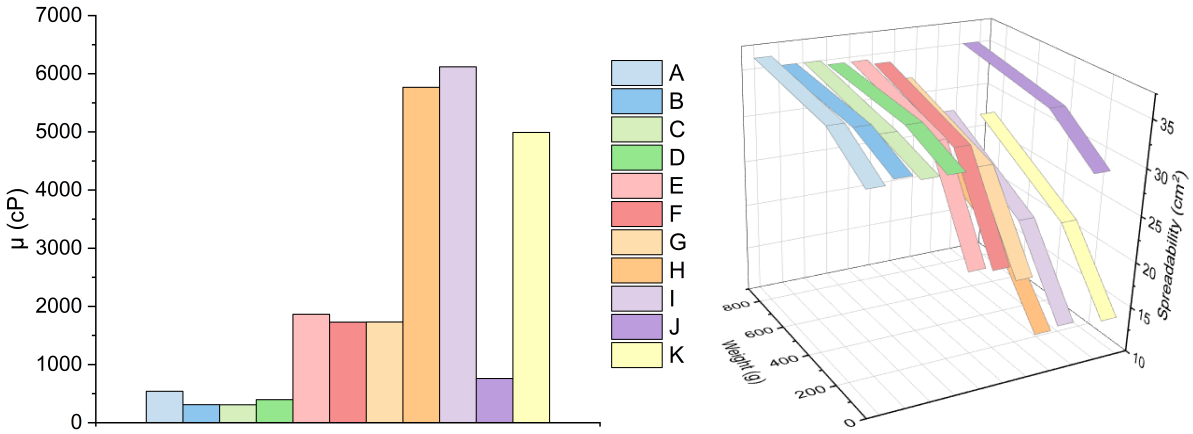

Figure 4.3: Viscosity (left) and spreadability (right) of the different hydrogel formulations.

the idea that formulations A, B, C and D are probably not suitable for this hydrogel-nanoparticle system.

The rest of the formulations macroscopically look good and homogeneous. The viscosity and spreadability of formulations E, F, G and J can be considered in the lower-medium range, between 1,000 and 2,000 cP. For formulations H, I and K the viscosity was high, around 5,000 and 7,000 cP, and the spreadability low. This happens because with the increase in viscosity, more force is needed to spread the

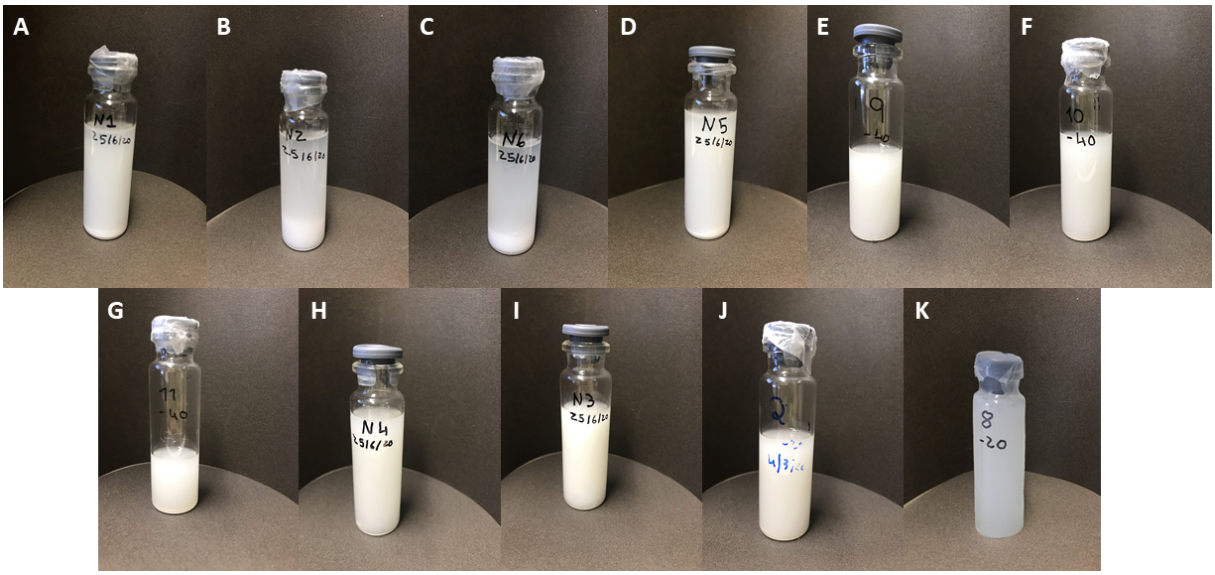

Figure 4.4: Photos of the different hydrogels. From left to right and up to down: A, B, C, D, E, F, G, H, I, J, K.

hydrogel, compared to more fluid formulations. The relationship between viscosity and spreadability is like described, the more viscous the formulation, the less it spreads, and vice versa.

The relation between these results and the hydrogel composition will be discussed in the next section 4.1.3.

4.1.3 Experimental design analysis

In order to better understand the relations between each independent variable, alginate, chitosan, glycerin and number of freeze-thawing cycles, and the dependent variables, mean particle size, zeta potential, viscosity and spreadability, these results were correlated in the Statistica program. The program returned with the relation that each dependent variable had with the independent variables. These results are shown in the following sections.

Mean particle size

For this dependent variable the relations given by the program are shown in Figures 4.5 and 4.6.

The p value indicates the evidence for the null hypothesis. The null hypothesis is a statistical theory that suggests that no statistical relationship and significance exists in a set of measured phenomena [89]. If the p value is less than 0.05, it indicates strong evidence against the null hypothesis, therefore suggesting a statistical and significance relationship between the variables. If the p value is greater than 0.05, there is a greater than 5% chance of the null hypothesis being correct, therefore considering the effect not statistically significant.

The F-statistic is another statistic test, that corroborates with the p-value. In order to reject the null hypothesis, and considering a statistical significance, the F value needs to be high [90].

In Figure 4.5 it is shown that for this model and data, none of the independent variables are statis-

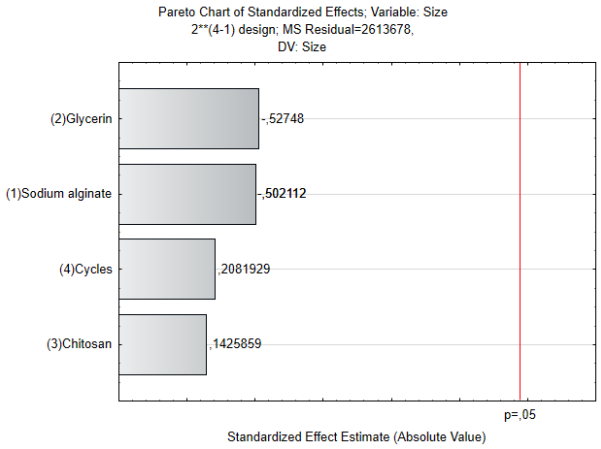

Factor	F	P
Sodium Alginate	0.252117	0.633479
Glycerin	0.278235	0.616787
Chitosan	0.020331	0.891285
Cycles	0.043344	0.841966

Figure 4.5: Pareto chart and analysis table of variation for ANOVA for the dependent variable, mean particle size.

tically significant for the outcome of the mean particle size. This is seen in the pareto chart were none of the variables reaches a p value of 0.5, and in the table of ANOVA variance. In this, the value of F is small, which is considered to mean that there is no statistic significance. The p values are all above 0.05, which also suggests no statistical significance.

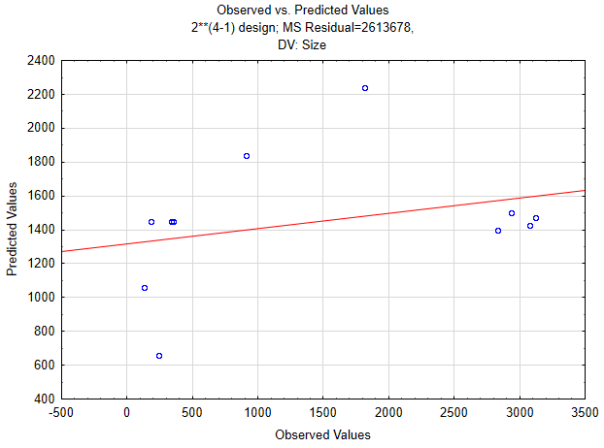

Figure 4.6: Observed vs Predicted graph for mean particle size dependent variable, R^2=0.09.

In Figure 4.6 it is shown a graph with the observed versus predicted values for the mean particle size variable. This Figures corroborates what was presented before, no independent variable is statistically significant and consequently the data in the graph is not linear with a really low R^2, which means the model cannot predict the mean particle size in function of the independent variables.

Zeta potential

For this dependent variable the relations given by the program are shown in Figures 4.7 and 4.8.

In Figure 4.7 it is shown that for this model and data, only sodium alginate is considered statistically significant for the outcome of the zeta potential. This is seen in the pareto chart were only sodium alginate reaches the p value line, and in the table of ANOVA variance where the F value is bigger than

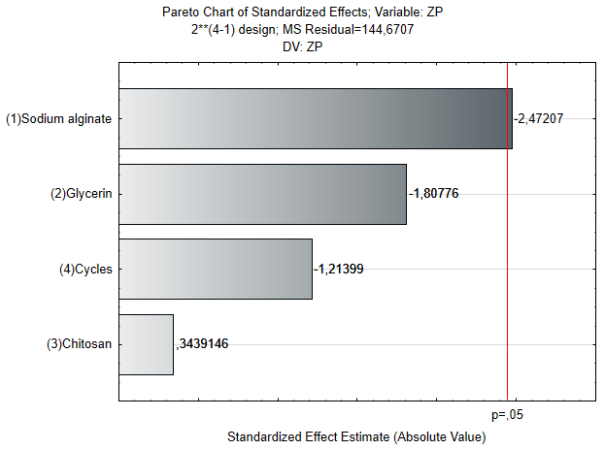

Factor	F	P
Sodium Alginate	6.111129	0.048322
Glycerin	3.267982	0.120649
Chitosan	0.118277	0.742643
Cycles	1.473770	0.270363

Figure 4.7: Pareto chart and analysis table of variation for ANOVA for the dependent variable, zeta potential.

the rest and the p value less than 0.05. This suggests the statistical significance of sodium alginate in the dependent variable.

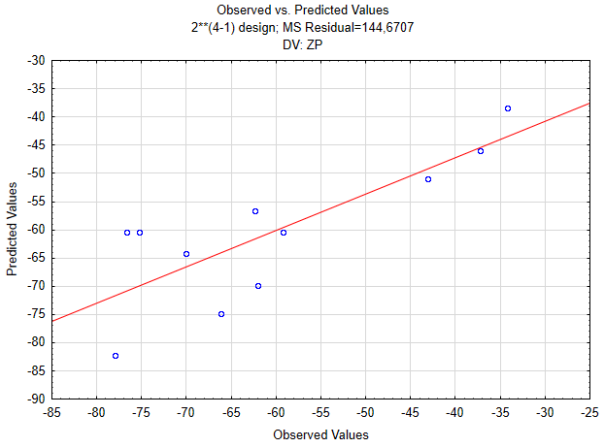

Figure 4.8: Observed vs Predicted graph for zeta potential dependent variable, R^2=0.646.

In Figure 4.8 it is shown a graph with the observed versus predicted values for the zeta potential variable. In this Figure the data is considered non-linear again with a low R^2 = 0.646, meaning the model cannot predict zeta potential values based on the independent variables.

Considering that sodium alginate is statistically significant and that chitosan is positively charged it is interesting to look at the fitted surface graph of these two independent variables and zeta potential. Figure 4.9 shows these correlations.

By analysing Figure 4.9, with the increase of chitosan composition the ZP slightly increases. This is to be expected since chitosan has a positive charge and the reason this is not more significant is that the data here is referred after gelification, when the sodium alginate has already masked the chitosan charge effect. Looking at the effect of sodium alginate, the zeta potential decreases with the increase in sodium alginate concentration in the formulation, another expected result due to the negative charge of sodium alginate.

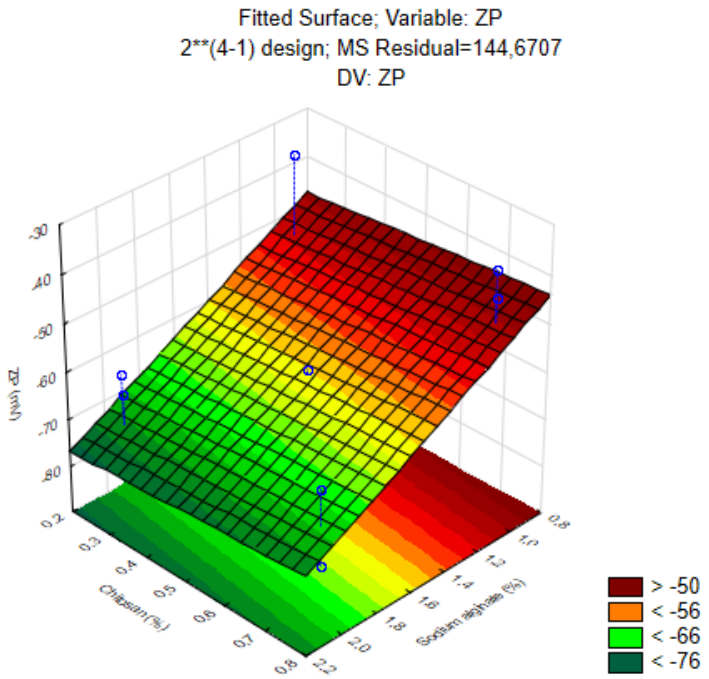

Figure 4.9: Fitted surface graph for zeta potential dependent variable and chitosan and sodium alginate.

Viscosity

For this dependent variable the relations given by the program are shown in Figures 4.10 and 4.11.

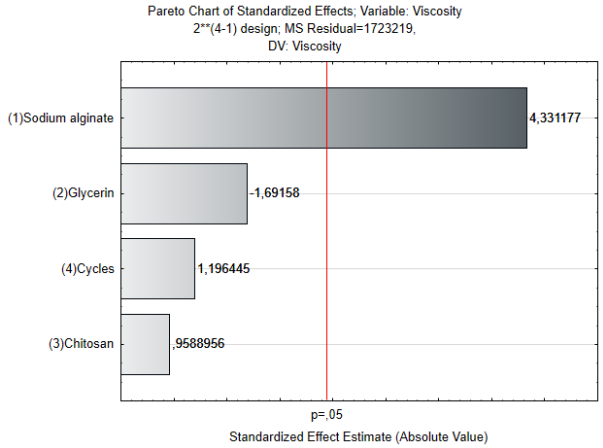

Factor	F	P
Sodium Alginate	18.75909	0.004922
Glycerin	2.86145	0.141677
Chitosan	0.91948	0.374640
Cycles	1.43148	0.276652

Figure 4.10: Pareto chart and analysis table of variation for ANOVA for the dependent variable, viscosity.

In Figure 4.10 it is shown that for this model and data, only sodium alginate is considered statistically significant for the outcome of the viscosity, because it is the variable that most contributes to the hydrogel properties, like viscosity. This is seen in the pareto chart were only sodium alginate surpasses a p value of 0.5, and in the table of ANOVA variance where the F value is much bigger than the rest and in the p value which is less than 0.05, suggesting the statistical significance of sodium alginate in the dependent variable.

In Figure 4.11 it is shown a graph with the observed versus predicted values for the viscosity variable. In this Figure the data is considered non-linear again with a bigger R^2, but still not acceptable for a

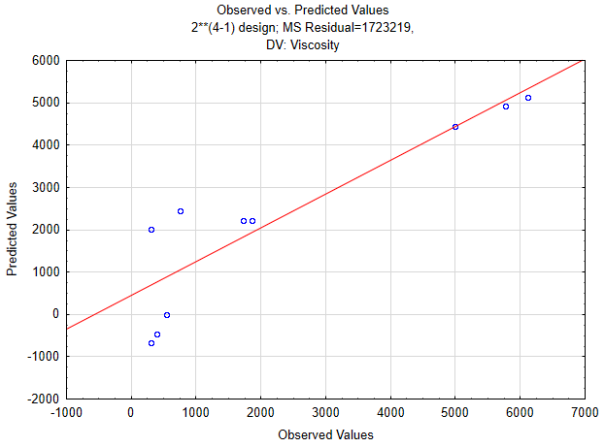

Figure 4.11: Observed vs Predicted graph for viscosity dependent variable, R^2=0.7998.

linear model. This means the model cannot perfectly predict viscosity values based on the independent variables.

Considering that sodium alginate is statistically significant and that the number of freeze-thawing cycles are supposed to increase the consistency of the formulation and also that glycerin by its liquid form could alter the formulation consistency, it is interesting to look at the fitted surface graph of these three independent variables and viscosity. Figure 4.12 shows these correlations.

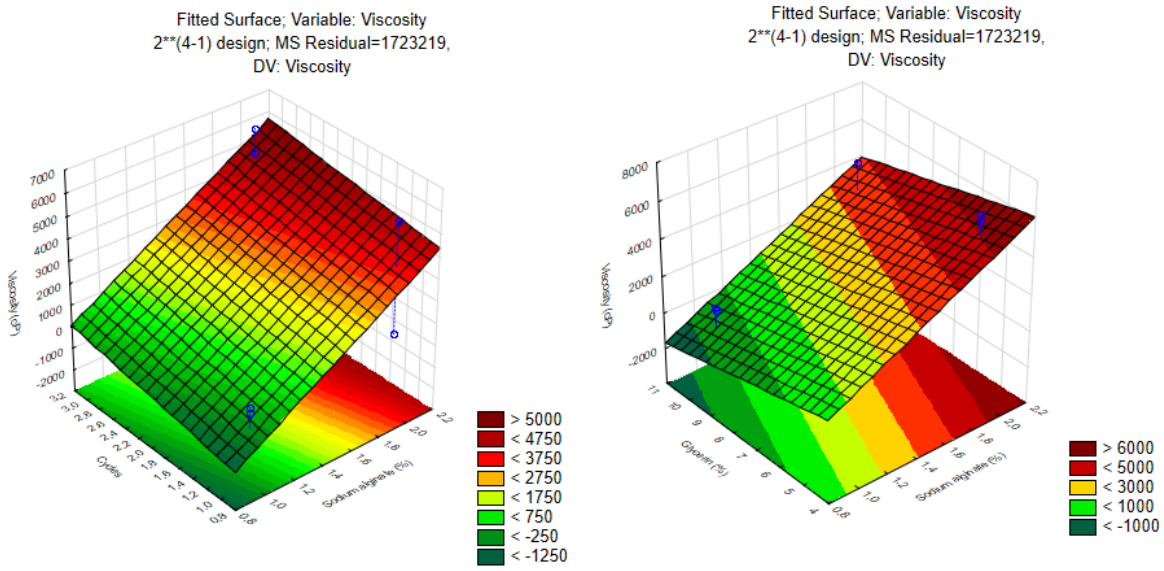

Figure 4.12: Fitted surface graph for viscosity dependent variable and sodium alginate with cycles and glycerin.

By analysing Figure 4.12, with the increase in the number of freeze-thawing cylces, the viscosity increases slightly. This is to be expected since the freeze-thawing cycles are supposed to make crooslinking reactions with water and PVA, causing gelation due to the formation of semi crystalline structures. This also justifies why this parameter does not have more effect in the viscosity of the formulations, since the formulations have in fact 2% PVA, but this is a fixed parameter in all formulations. Since the concentration of PVA does not vary, the correlations between the number of freeze-thawing cycles and

viscosity are not easily seen, causing it to be less significant in the viscosity outcome.

In terms of the effect of glycerin in the viscosity, with the increase of glycerin concentration the viscosity decreases, which is to be expected since the glycerin is used in the hydrogel as an emollient.

Looking at the effect of sodium alginate, the viscosity increases with the increase in sodium alginate concentration in the formulation, another expected result due to the alginate gelation properties in aqueous solutions [91].

Spreadability

For this dependent variable the relations given by the program are shown in Figures 4.13 and 4.14.

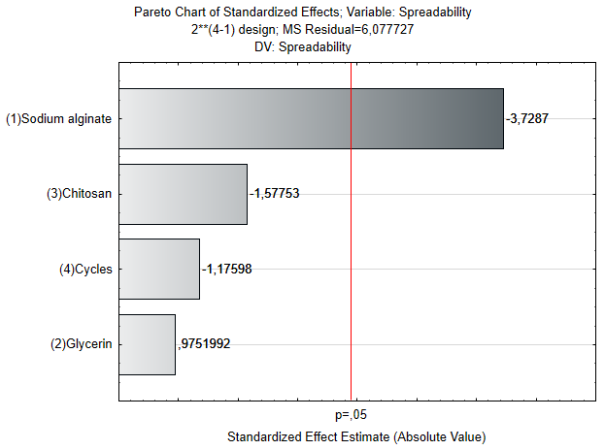

Factor	F	P
Sodium Alginate	13.90322	0.009752
Glycerin	0.95101	0.367123
Chitosan	2.48859	0.165749
Cycles	1.38292	0.284147

Figure 4.13: Pareto chart and analysis table of variation for ANOVA for the dependent variable, spreadablity.

In Figure 4.13 it is shown that for this model and data, only sodium alginate is considered statistically significant for the outcome of the spreadability. This is seen in the pareto chart were only sodium alginate surpasses a p value of 0.5, and in the table of ANOVA variance where the F value is much bigger than the rest and in the p value which is less than 0.05, suggesting the statistical significance of sodium alginate in the dependent variable.

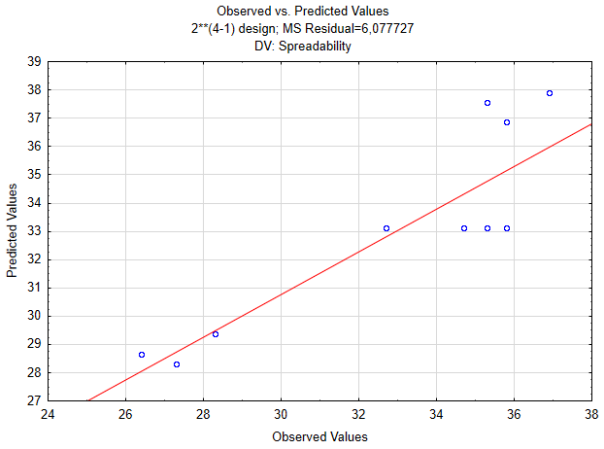

Figure 4.14: Observed vs Predicted graph for spreadability dependent variable, R^2=0.757.

In Figure 4.14 it is shown a graph with the observed versus predicted values for the spreadability variable. In this Figure the data is considered non-linear again with R^2=0.757, still considered not acceptable for a linear model. This means the model cannot perfectly predict spreadability values based on the independent variables.

Considering that sodium alginate is statistically significant and that the number of freeze-thawing cycles and chitosan composition are supposed to alter the consistency of the formulation, it is interesting to look at the fitted surface graph of these three independent variables and spreadability. Figure 4.15 shows these correlations.

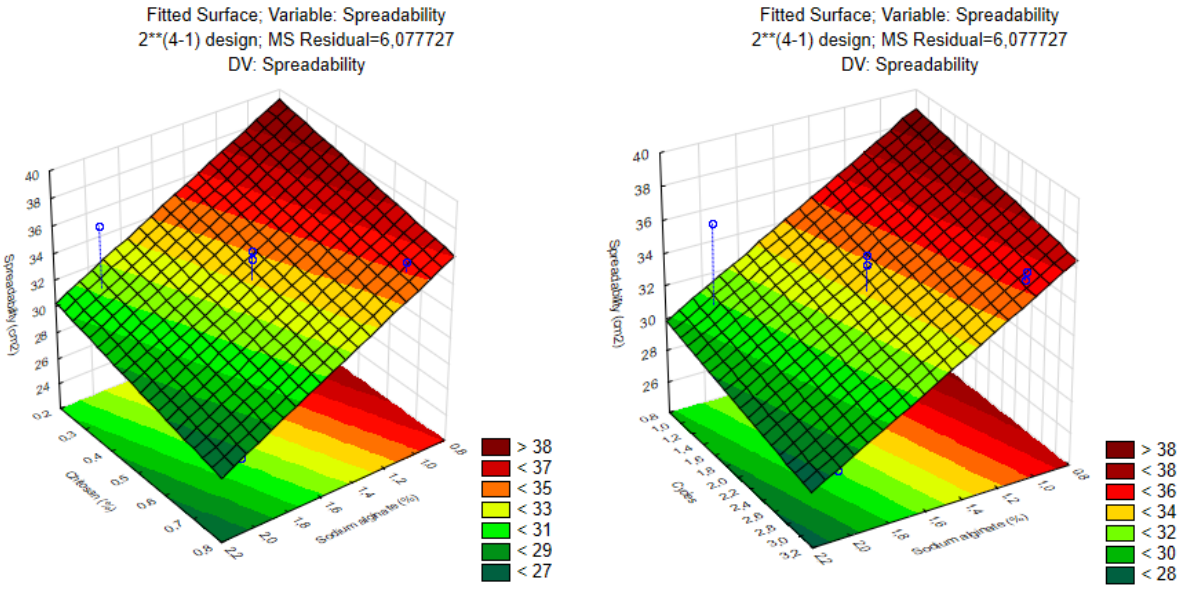

Figure 4.15: Fitted surface graph for viscosity dependent variable and sodium alginate with cycles and chitosan.

By analysing Figure 4.15, with the increase in the number of freeze-thawing cycles, the spreadability decreases slightly. This is similar to the results from the viscosity, which is understandable since the two are relatable.

In terms of the effect of chitosan in the spreadability, with the increase of chitosan concentration the spreadability decreases. This is probably justified by the chitosan muco-adhesive properties, that prevent the over spreading of the hydrogel [65].

Looking at the effect of sodium alginate, the spreadability decreases with the increase in sodium alginate concentration in the formulation, another result similar to viscosity due to the alginate gelation properties.

Optimal hydrogel formulation

In order to obtain the optimal hydrogel formulation, the constraints of each variable were given to the Design-Expert program, and the list of these factors is presented in Table 4.2.

For the sodium alginate was given a goal to maximize its concentration, with a maximum of 2%. This is because the ability of alginate of absorbing excess fluid in the wound bed is very important

Table 4.2: Constraints given to the program to obtain the optimal formulation relative to all variables, dependent and independent.

Name	Goal	Lower Limit	Upper Limit
Sodium alginate	Maximize	1	2
Glycerin	In range	5	10
Chitosan	Maximize	0.25	0.75
Cycles	In target = 1	1	3
Mean particle size	In range	133	3123
Zeta potential	In range	-78	-34.2
Viscosity	In range	1000	6120
Spreadability	In range	26.4	35

and it was a property worth maximizing. The glycerin had a goal of keeping in the range of 5-10%. The reason for this is that the function in the hydrogel is to serve as a bodying agent, and therefore, keeping the range allows the program to decide the better concentration for the desired outputs, mainly the viscosity. The chitosan was chosen to maximize in the value of 0.75%, in order to obtain the best muco-adhesion properties possible. The number of cycles was targeted to just one cycle due to energy and time consumption and because this variable did not had a relevant influence with the dependent variables.

For the dependent variables of mean particle size and zeta potential both were given the goal of keep the results in range, since all these results were in conformation with what was expected. Since there was certain formulations that did not have an acceptable macroscopic look, less colloidal stability, the goal for the viscosity was to keep the range of around 1,000-10,000 cP. This is typically the better range for topical application [87, 88] and a range that the results showed to have an acceptable macroscopic look with good colloidal stability. For the spreadability, the goal was to range in between the results obtained previously, since the spreadability does not directly affect the colloidal stability, and so it was let to the program to decide the better glycerin concentration.

Given the constraints, the solution for the optimal formulation given by the program was 2% sodium alginate, 6% glycerin, 0.75% chitosan and 1 freeze-thawing cycle. This composition will be used for the remaining tests ahead, where insulin will be loaded in the nanoparticles.

4.2 Insulin-loaded nanoparticle-hydrogel characterization

The optimal formulation that resulted from the design experiment approach is the one used for the tests with insulin loaded nanoparticles.

4.2.1 Nanoparticles Characterization

To begin the insulin-loaded nanoparticle-hydrogel characterization, using the optimal formulation obtained by design of experiments, the effect of insulin association needs to be evaluated in the nanoparticles characteristics. In order to understand the effects of insulin and chitosan in the characterization

of the nanoparticles, four experimental groups were used: PLGA nanoparticles (PLGA Np), chitosan-coated PLGA nanoparticles (Chi-PLGA Np), insulin-loaded PLGA nanoparticles (Ins-PLGA Np) and insulin-loaded chitosan-coated PLGA nanoparticles (Ins-Chi-PLGA Np).

For this the mean insulin loaded nanoparticles size, PdI and zeta potential after production were assessed and the results are shown in Figure 4.16.

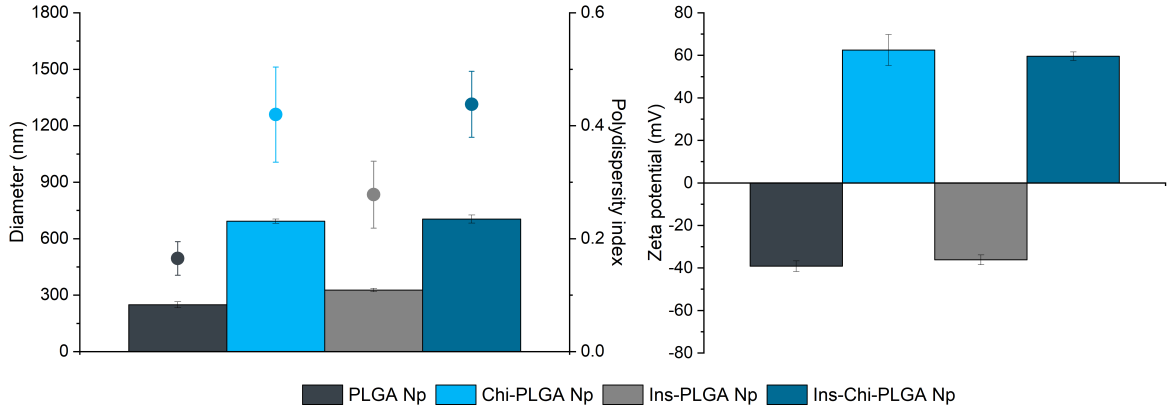

Figure 4.16: Mean particle size (left bars), polydispersity index (interval plot) and zeta potential (right bars) characterization of PLGA Np, chitosan-coated PLGA Np, insulin-loaded PLGA Np and insulin-loaded chitosan-coated PLGA Np all with 0.75% chitosan (n=3, mean $\pm$ SD).

The results show an increase in the diameter for the chitosan coated nanoparticles, when compared to the uncoated. This was expected, as it happened in section 4.1.1, the chitosan attached to the nanoparticles, creating a thicker layer around the surface of the nanoparticles and thus creating an increase in the size of the nanoparticles. As showed, the insulin encapsulation did not significantly influence the size of the nanoparticles. The mean particle size values were 248.6$\pm$15.7 nm, 693.3$\pm$11.4 nm, 326.9$\pm$9.0 nm and 704.3$\pm$21.2 nm for PLGA nanoparticles, chitosan-coated PLGA nanoparticles, insulin-loaded PLGA nanoparticles and insulin-loaded chitosan-coated PLGA nanoparticles, respectively.

The zeta potential values were -39.2$\pm$2.5 mV, 62.5$\pm$7.3 mV, -36.2$\pm$2.3 mV and 59.6$\pm$2.0 mV for PLGA nanoparticles, chitosan-coated PLGA nanoparticles, insulin-loaded PLGA nanoparticles and insulin-loaded chitosan-coated PLGA nanoparticles, respectively. These values show a change in the coated nanoparticles, exhibiting a positive zeta potential, as opposed to the uncoated nanoparticles.

The results from the diameter and the zeta potential corroborate the effective chitosan coating, already explained in section 4.1.1.

The values of PdI were low enough to be considered homogenous samples. The values were 0.165$\pm$0.03, 0.420$\pm$0.08, 0.278$\pm$0.06 and 0.438$\pm$0.06 for PLGA nanoparticles, chitosan-coated PLGA nanoparticles, insulin-loaded PLGA nanoparticles and insulin-loaded chitosan-coated PLGA nanoparticles, respectively.

In Table 4.3 the AE and LC results are presented. The AE was evaluated to assess the insulin association efficiency, an information very important to have in order to know the amount of insulin in the nanoparticles, especially to use in further tests, like in section 4.3.1, for the insulin release profile. The

Table 4.3: Association efficiency and loading capacity results for insulin-loaded chitosan-coated PLGA Np hydrogel and insulin-loaded PLGA Np hydrogel (n=3, mean ± SD).

Formulation	Association efficiency (%)	Loading Capacity (%)
Ins-Chi-PLGA Np	92.95 ± 1.76	12.12 ± 0.23
Ins-PLGA Np	93.22 ± 0.36	12.15 ± 0.05

LC was used to know the insulin loading capacity of the nanoparticles. The association efficiency was above 90% for both formulations, a very good result, taking into account the hydrophilic nature of insulin and hydrophobic polymeric nanoparticles. The results for AE and LC are in conformation to previous studies [92].

4.2.2 Hydrogel Characterization

To continue the insulin-loaded nanoparticle-hydrogel characterization, using the optimal formulation obtained by design of experiments, the effect of insulin association needs to be evaluated in the hydrogel characteristics. In order to understand the effects of insulin and chitosan in the characterization of the hydrogel, five experimental groups were used: insulin-loaded chitosan-coated PLGA nanoparticle-hydrogel (Ins-Chi-PLGA Np-hydrogel), insulin-loaded PLGA nanoparticle-hydrogel (Ins-PLGA Np-hydrogel), chitosan-coated PLGA nanoparticle-hydrogel (Chi-PLGA Np-hydrogel), PLGA nanoparticle-hydrogel (PLGA Np-hydrogel) and hydrogel without nanoparticles (blank hydrogel).

The hydrogel characteristics were evaluated using the gelification ratio and zeta potential after gelification, to evaluate whether the nanoparticle size and zeta potential changed after insulin loading and gelification, and the water content. These results are shown in Table 4.4.

Table 4.4: Gelification ratio, water content and ZP after gelification for the different hydrogel formulations: of insulin-loaded chitosan-coated PLGA Np hydrogel, insulin-loaded PLGA Np hydrogel, chitosan-coated PLGA Np hydrogel, PLGA Np hydrogel and hydrogel without nanoparticles (n=3, mean ± SD).

Formulation	Gelification Ratio	Water content (%)	ZP (mV)
Ins-Chi-PLGA Np-hydrogel	0.95 ± 0.13	89.2 ± 0.1	-12.9 ± 1.6
Ins-PLGA Np-hydrogel	1.42 ± 0.23	88.6 ± 0.2	-53.0 ± 6.0
Chi-PLGA Np-hydrogel	1.27 ± 0.17	89.3 ± 0.2	-9.5 ± 1.3
PLGA Np-hydrogel	1.55 ± 0.15	88.7 ± 0.3	-56.1 ± 2.1
Blank hydrogel	-	89.9 ± 0.1	-

The gelification ratio divides the mean particle size after gelification by the mean particle size before gelification, to assess the changes in the size of the nanoparticles after gelification. If the gelification ratio is greater than 1, the nanoparticles size increased, which can indicate particle aggregation upon gelification. If the ratio is less than 1, the nanoparticles could have suffered fragmentation in the gelification process. If the ratio is equal to 1, the nanoparticles did not suffer size alterations.

In the results given in Table 4.4 the gelification ratio was close to the unit in all the formulations, but a bit higher in the formulations without chitosan coating, suggesting that there might have been particle agglomeration in these samples. The fact that the chitosan coated nanoparticles had a gelification ratio

closer to 1 further addresses the advantages of the presence of the chitosan coating in the delivery system.

The water content in all formulations was around 89%, which was expected for a hydrogel. The high water content is very beneficial to provide a moist environment to the wound bed, promoting tissue regeneration. The zeta potential values are all negative showing a change from positive to negative values in the formulations with chitosan coating that conferred them a positive charge after production, and that now are negative from the alginate present in the hydrogel. Like in section 4.1.1, the sodium alginate camouflaged the chitosan, changing the surface charge of the nanoparticles. Another interesting find was the fact that the uncoated nanoparticles showed a more negative zeta potential value, which is expected, since these nanoparticles did not had the chitosan to compensate the surface charge to a more positive value.

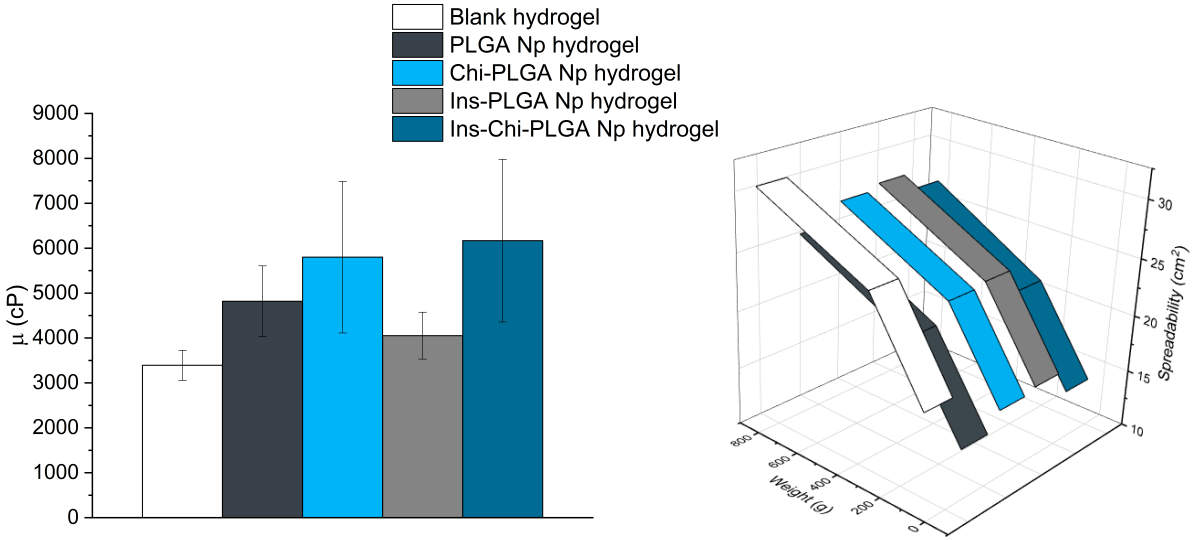

Figure 4.17: Viscosity and spreadability after 1 freeze-thawing cycle for blank hydrogel, PLGA Np hydrogel, chitosan-coated PLGA Np hydrogel, insulin-loaded PLGA Np hydrogel and insulin-loaded chitosan-coated PLGA Np hydrogel.

In Figure 4.17 the viscosity and spreadability results show that the formulations with chitosan coating were seen to have a tendency of a higher viscosity, although probably not statistically significant. This tendency was not observed in the spreadability of the formulations, with all showing relatively approximate results for the spreadability. All samples showed a proper viscosity range for topical application (1,000-10,000 cP).

In Figure 4.18 photos of the different hydrogels are shown. Macroscopically all look acceptable, with no signs of deposits in the bottom, which conveys good uphold of the nanoparticles in the hydrogel and good colloidal stability. Additionally, the hydrogels with nanoparticles feature a milky aspect, typical from the nanoparticles, and this is not shown in the blank hydrogel.

To evaluate the nanoparticle physiognomy, SEM images where obtained. To assess the changes that happen when the nanoparticles are embedded in the hydrogel, and after the gelification, SEM images where taken in tree different stages of the production process: after production of the nanoparticles (Np after production), nanoparticles embedded in the hydrogel (Np loaded hydrogel), nanoparticles removed

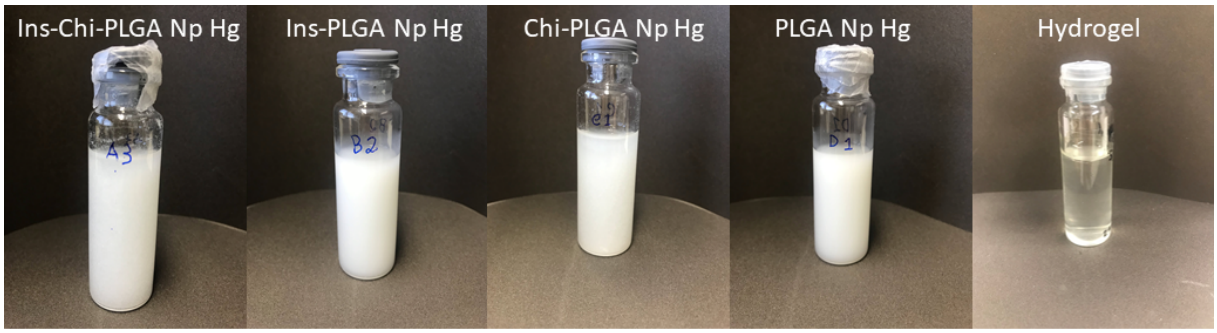

Figure 4.18: Photos of the different hydrogels. From left to right: insulin-loaded chitosan-coated PLGA Np hydrogel, insulin-loaded PLGA Np hydrogel, chitosan-coated PLGA Np hydrogel, PLGA Np hydrogel and hydrogel without nanoparticles.

from the hydrogel, after gelification (Np in hydrogel).

In Figure 4.19 SEM images are shown. In the after production phase it is possible to acknowledge that the nanoparticles have a characteristic round shape and smooth surface. It is not possible to see a difference between the different nanoparticles, which indicates that insulin encapsulation does not alter the physiognomy of the nanoparticles. In the nanoparticle loaded hydrogel, although the hydrogel matrix is overlapping the nanoparticles, it is possible to see that the nanoparticles are really well embedded in the hydrogel, which corroborates with the macroscopic assay (Figure 4.18). In the nanoparticles in hydrogel column, the nanoparticles were removed from the hydrogel in order to assess their conformation after the gelification process. The nanoparticles show no modification comparing to after production, they remain round and with a smooth surface, which suggests that the gelification process did not alter the nanoparticles conformation. However, there is a difference to be noted, the nanoparticles coated with chitosan appear to have the chitosan coating still embedded around the nanoparticles. This also means that the chitosan coating remained attached in the nanoparticles after centrifugation for hydrogel removal. This is supported by the presence of a strong electrostatic interaction between the PLGA from the particles and the chitosan coating them, due to their opposite charges - PLGA with negative surface charge and the chitosan with positive. In all the different phases of the production, the nanoparticles maintained their integrity and the size was in accordance with those from Figure 4.16.

Fourier-transform infrared spectroscopy

FTIR spectroscopy was used to assess the predominant interactions between the different constituents of the nanoparticle-hydrogel formulation. The FTIR spectra are shown in Figure 4.20.

The formulations analysed were the hydrogel without the nanoparticles (Hydrogel), insulin-loaded nanoparticle-hydrogel (Ins-Np-H) and the chitosan-coated insulin-loaded nanoparticle-hydrogel (Chi-Ins-Np-H). From Figure 4.20, it is possible to see that the spectra from the nanoparticle-hydrogel is very similar to the spectra from the the hydrogel without the nanoparticles. This demonstrates that the predominant interactions between the different constituents of the formulation are the ones that allowed the production of the hydrogel by freeze-thawing. This means that the interactions between the nanoparticles and the hydrogel are not evident, and are probably masked by the hydrogel interactions. These

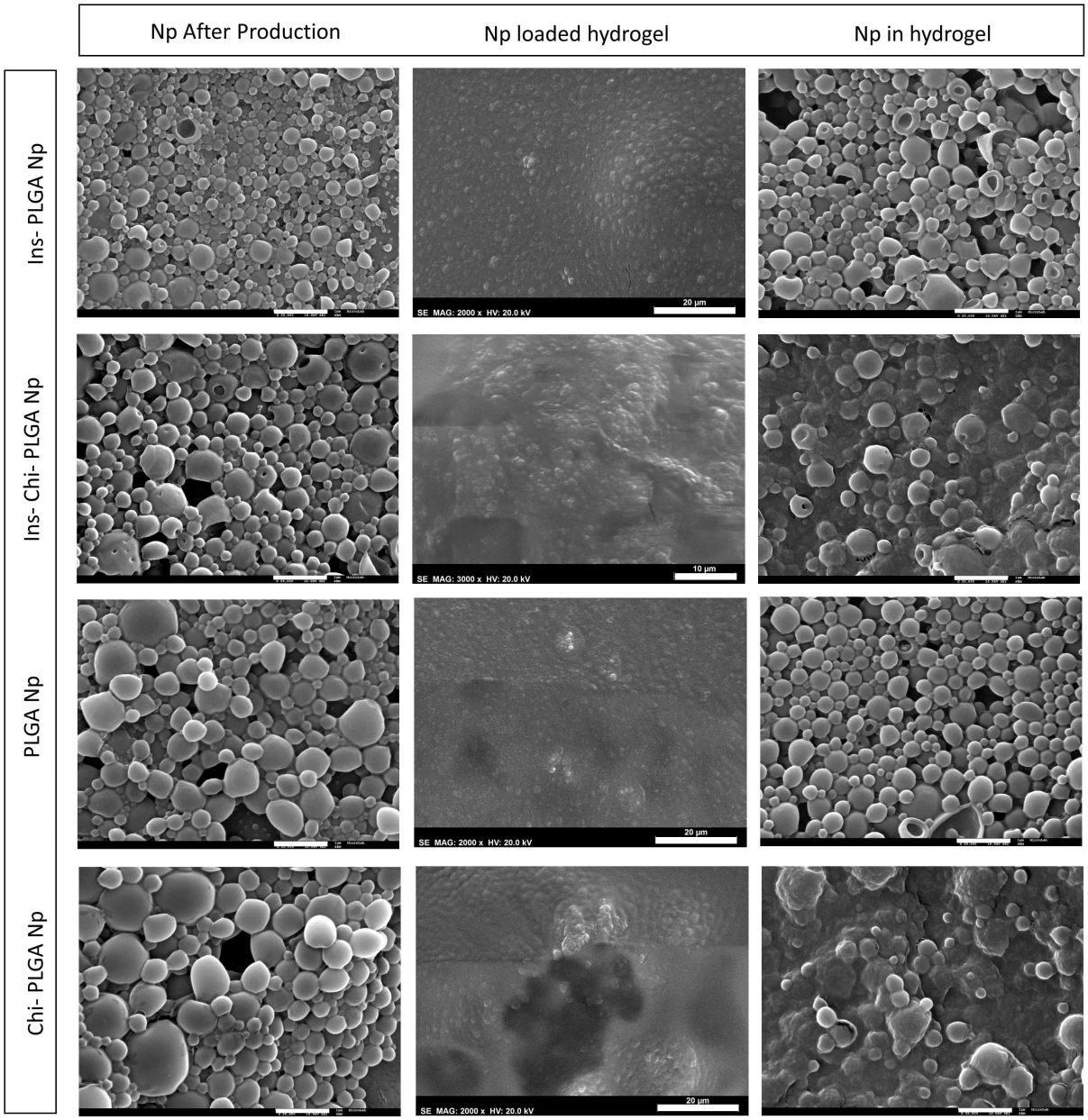

Figure 4.19: Nanoparticles-hydrogel SEM images. Insulin-loaded PLGA Np, insulin-loaded chitosan-coated PLGA Np, PLGA Np and chitosan-coated PLGA Np (from top to bottom), after NP production and nanoparticles after gelification with and without hydrogel (left to right). Scale bar: 1 μm for first and third column, 10 μm for second picture of second column and 20 μm for the rest of the second column .

results support the claim that the hydrogel confers a good matrix to contain the nanoparticles without altering their characteristics.

4.2.3 Protein Structure Assessment

After all the nanoparticle and hydrogel appraisal, the insulin structure from the loaded nanoparticles was assessed. For this, the insulin was extracted from the hydrogel nanoparticle like described in section 3.5.1, in order to assess the insulin structure and its bioactivity, after the nanoparticle-hydrogel production.

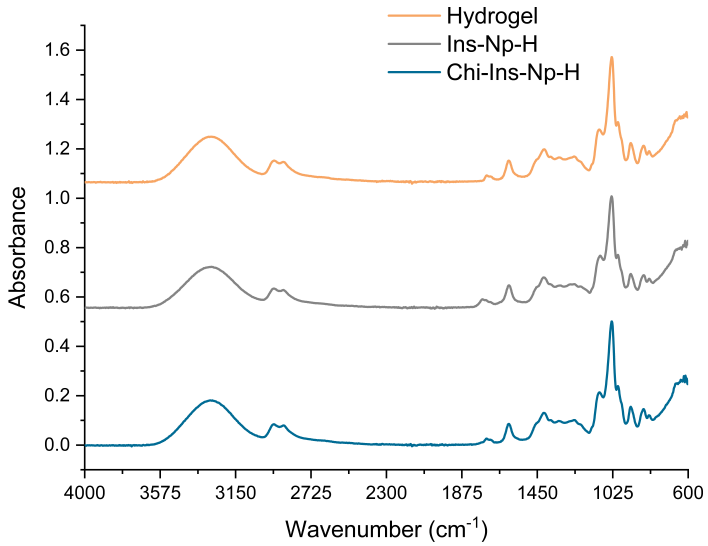

Figure 4.20: FTIR spectra of liofilized insulin-loaded chitosan-coated PLGA nanoparticles hydrogel, insulin-loaded PLGA nanoparticles hydrogel and hydrogel without nanoparticles. Insulin 0.2 mg/mL in 0.01 HCl used as reference.

Thioflavin T assay

Thioflavin T is a cationic benzothiazole dye that exhibits enhancement of fluorescence at 485 nm when bind to amyloid fibrils with crossed β-sheet structures. The presence of these amyloid fibrils means the protein structure and its bioactivity is compromised. Insulin may form these protein aggregates due to various stress factors, so assessing this is very important to understand if the protein structure remains unaltered. If there is no signal intensification, insulin is not aggregated, otherwise, if there is signal intensification the insulin is aggregated [93]. The positive control is a insulin solution heated at 60°C overnight to denaturate and form fibrils. The negative control is a insulin solution prepared fresh in the moment.

Table 4.5: Thioflavin assay for insulin-loaded chitosan-coated PLGA Np hydrogel, insulin-loaded PLGA Np hydrogel, chitosan-coated PLGA Np hydrogel, PLGA Np hydrogel, positive and negative control (n=3, mean $\pm$ SD). Insulin extracted from the nanoparticles.

Formulation	**Thioflavin T assay**
Ins-Chi-PLGA Np-hydrogel	-0.31 $\pm$ 0.12
Ins-PLGA Np-hydrogel	-0.33 $\pm$ 0.19
Chi-PLGA Np-hydrogel	-0.19 $\pm$ 0.24
PLGA Np-hydrogel	-0.23 $\pm$ 0.16
Positive Control	92.7 $\pm$ 0.34
Negative Control	0.029 $\pm$ 0.27

Thioflavin T assay results are shown in Table 4.5. All samples showed no signal enhancement, which means no presence of thioflavin T positive filaments or formation of amyloid fibrils. The positive control showed signal enhancement which is expected since this was fibrillated insulin. These results show that the production method maintained the insulin structure stable.

Circular Dichroism

In order to further test the secondary structure of insulin CD spectroscopy was performed. The spectra obtained are shown in Figure 4.21.

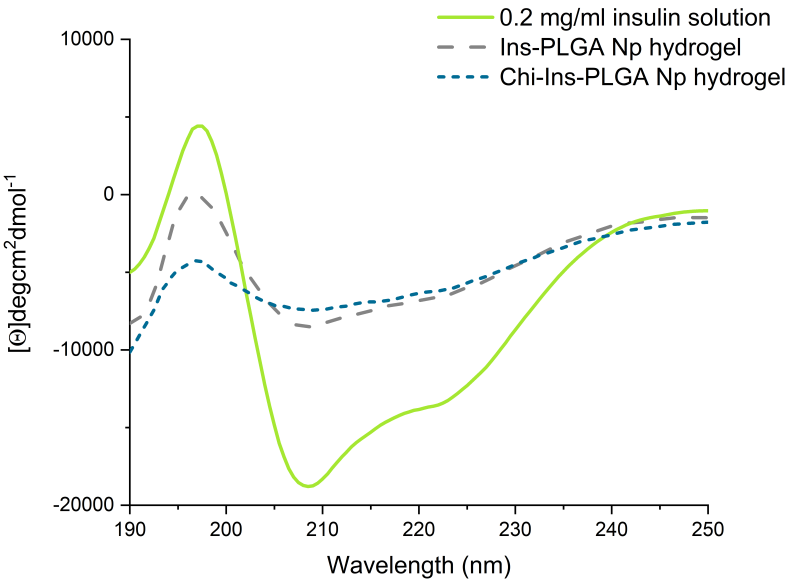

Figure 4.21: Far-UV CD spectra of insulin extracted from insulin-loaded PLGA nanoparticles hydrogel and insulin-loaded chitosan-coated PLGA nanoparticles hydrogel. Insulin 0.2 mg/mL in 0.01 HCl used as reference.

The reference spectra used is native insulin at 0.2 mg/ml. In this, two minima were observed at 208.5 and 222 nm, which are distinct of the α-helix structure of the protein [94]. A maximum was also observed at 197 nm. This spectra is in accordance with other described by research works [95].

The CD spectra from the samples showed a similar shape of the curve, with the two minina and maximum at about the same wavelength. Maximum at 197 nm for both samples, and minima at 209 and 222.5 nm for Ins-PLGA nanoparticle hydrogel and 208.5 and 221.5 nm for Chi-Ins-PLGA nanoparticle hydrogel. These results show no relevant changes in the α-helix structure.

As for the β-sheets, these are predominant if denaturation, aggregation or even fibrillation of insulin occurs. It is possible to observe this presence of β-sheets with a characteristic minima of ellipticity at around 216 nm [96]. Considering this is not observed in Figure 4.21, the structural modifications from α-helix into β-sheets did not occur, so it is predicted that the insulin extracted from the hydrogel-nanoparticle formulations maintained its secondary structure and bioactivity.

The differences observed in the CD spectra are related to the ellipticity signal, which represents some change in the spatial conformation of the protein. This is to be expected since the insulin extracted from the nanoparticles is exposed to some invasive procedures, like the production of the nanoparticles and hydrogel, and the extraction in itself. Besides the presence of this insulin conformation change, the maintenance of the minina suggest that the insulin maintained its bioactivity.

Fluorescence

Fluorescence spectroscopy was used to assess the structure of insulin extracted from PLGA nanoparticle hydrogel system. Insulin fluorescence depends on its four tyrosine residues, hence alterations in the intensity of the emission spectra of insulin are indicators of conformation modification [97]. The fluorescence spectra are shown in Figure 4.22

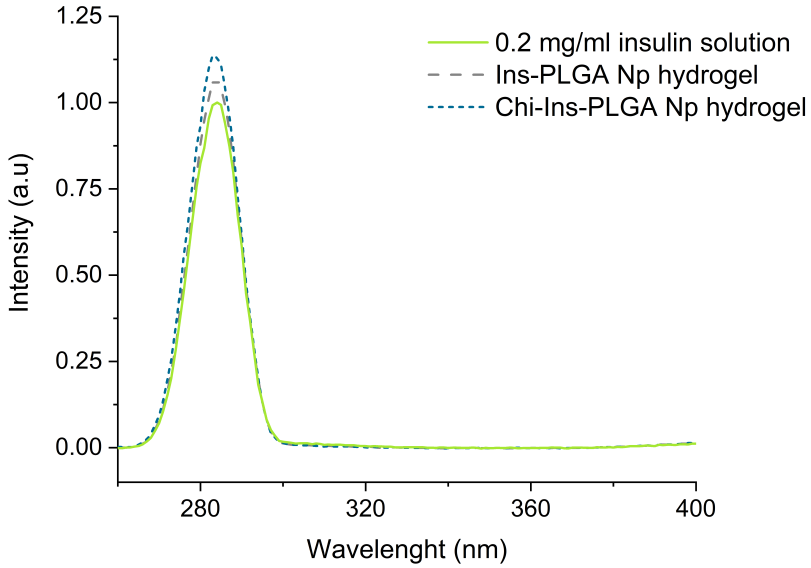

Figure 4.22: Fluorescence spectra of insulin extracted from insulin-loaded PLGA nanoparticles hydrogel and insulin-loaded chitosan-coated PLGA nanoparticles hydrogel. Insulin 0.2 mg/mL in 0.01 HCl used as reference.

For the reference insulin spectrum an insulin solution at 0.2 mg/ml was used. In this spectrum, and for the sample spectra a maximum was observed at 284 nm. This maximum is shifted when compared to the literature [98], however when comparing between the reference insulin spectrum and the samples spectra there is no shift in the maxima, which is an indication of the preservation of insulin structure. However there are some differences regarding the increase in intensity observed, which hints to some conformational changes [99]. Insulin from Ins-PLGA nanoparticle hydrogel showed higher intensity and insulin from Chi-Ins-PLGA nanoparticle hydrogel showed even higher intensity when compared to native insulin spectrum. Again, expected results due to the stress exposure of the insulin extracted from the samples. Overall, the results indicate a stable structure, and are in agreement with previous structural characterization results from CD and thioflavin T assay.

4.3 *In vitro* Results

4.3.1 Insulin release profile

To obtain an insulin release profile, the hydrogels containing insulin loaded nanoparticles, insulin-loaded chitosan-coated PLGA nanoparticles hydrogel (Chi-Ins PLGA Np-Hydrogel) and insulin-loaded PLGA

nanoparticles hydrogel(Ins PLGA Np-Hydrogel), were used in a release profile methodology for up to 72h. These results were obtained in order to understand the release rate of insulin from the nanoparticles embedded in the hydrogel. The profile obtained is represented in Figure 4.23.

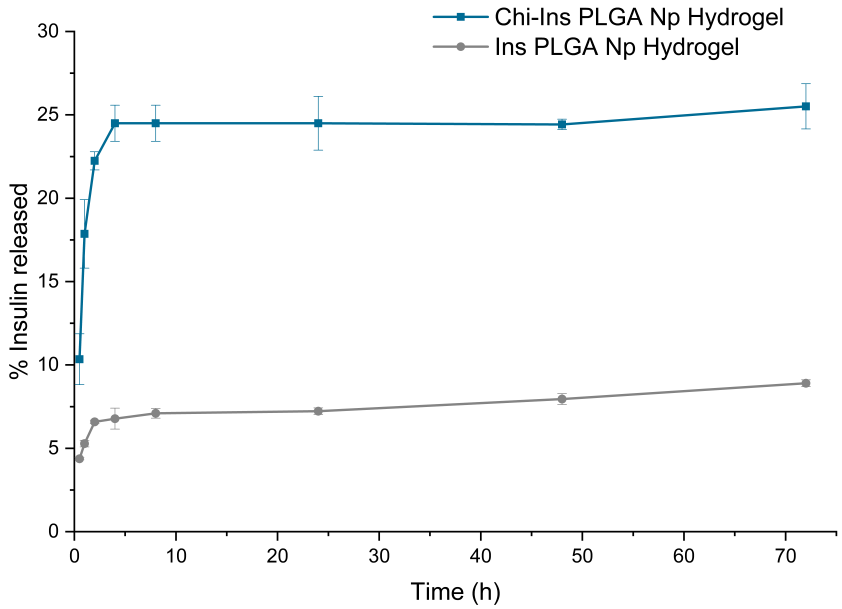

Figure 4.23: Insulin release profile from insulin-loaded chitosan-coated PLGA nanoparticles hydrogel and insulin-loaded PLGA nanoparticles hydrogel.

The insulin release profile shows the cumulative insulin release up to 72h, for the insulin-loaded chitosan-coated PLGA nanoparticle hydrogel and insulin-loaded PLGA nanoparticle hydrogel. The release pattern for both formulations is similar, with the difference in the amount of insulin released. The initial burst effect of insulin release in the first 4h is related to the existence of insulin in the surface of the nanoparticles, which facilitates the diffusion to the medium. From that moment on, the release of insulin is more controlled and steady. Until the 72h a sustained release pattern is observed, reaching about 10 and 25 % for insulin-loaded chitosan-coated PLGA nanoparticle hydrogel and insulin-loaded PLGA nanoparticle hydrogel, respectively. The pattern also indicates that the release of insulin should continue past the 72h, but it is not possible to confirm, without data with more time. The results also indicate that the nanoparticles with chitosan-coating released more insulin over time than the ones without. The reason for this is probably the higher muco-adhesive properties from the chitosan coating, that enables a more intimate interaction between the nanoparticles and the insert membrane, which promotes a greater insulin release. This particular result demonstrates the advantage of using chitosan coating in this delivery system. Furthermore, when comparing this release assay with others from insulin-loaded PLGA nanoparticles without the hydrogel [79], where the insulin was 100% released over 48h, the very obvious difference is the amount the insulin released. When the hydrogel is not present, the nanoparticles are free from the hydrogel matrix, and can release the insulin with more ease. Having the nanoparticles embedded in the hydrogel creates barrier for the release of insulin, which can be advantageous, if a more controlled and sustained release is needed.

4.3.2 Cell Scratch assay

To investigate the bioactivity of the insulin and the hydrogels with the nanoparticles, cell scratch assay was performed in MSC. These cells were used as a prove of concept to evaluate the regenerative properties of the hydrogel, but for future assays, HaCaT skin cells will be used. The area of the scratch was measured at the beginning of the experiment at 24, 36 and 48h. The empty area of the scratch over the time for each condition is represented in Figures 4.24 and 4.25.

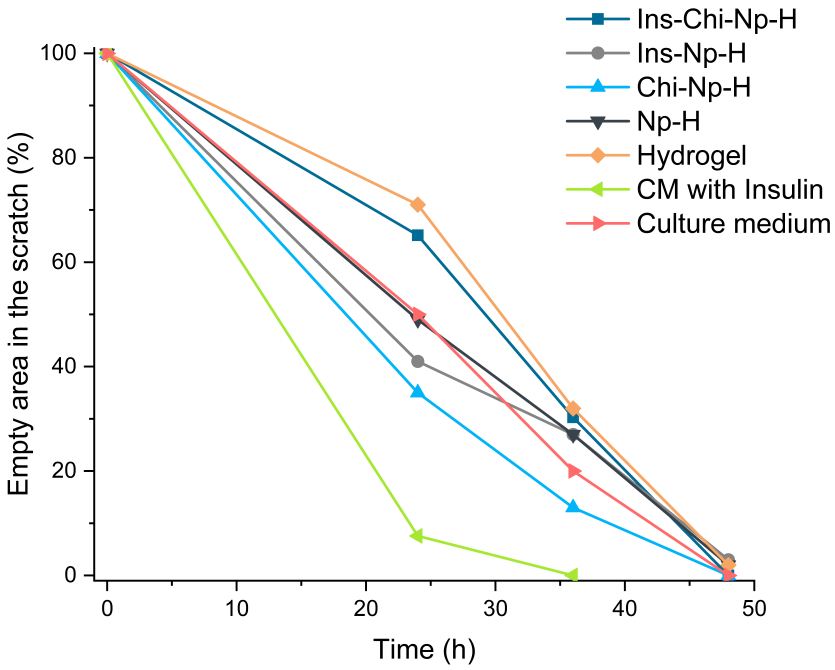

Figure 4.24: MSC cell scratch repair assays for evaluation of insulin's bioactivity from Ins-Chi-Np-H, Ins-Np-H, Chi-Np-H, Np-H, Hydrogel, MSC expansion culture medium supplemented with insulin 10^{-7} M and MSC expansion culture medium. CM stands for culture medium.

The scratch assay provides a measure of cell migration, a critical process for wound healing. The results show that insulin strongly stimulated cell migration, being the only condition that at 24h showed around 90% of the scratch closed and full closure at 36h. For all other conditions cell migration was not as evident, or significantly different between conditions. It was expected that the nanoparticles loaded with insulin would induce cell migration as well, but this was not observed. As seen in section 4.2.3, the insulin from the nanoparticles seemed to conserve its secondary structure, which should also indicate its bioactivity. Knowing this, the probable justification for the fact that the Ins-Chi-Np-H and Ins-Np-H conditions did not showed enhanced cell migration, when compared to the control conditions, could be that the insulin release from the nanoparticles, as seen in section 4.3.1, was not sufficient to induce cell migration. As seen in the insulin release assay, the insulin released in the Ins-Chi-Np-H and Ins-Np-H reached a maximum of 25 and 10 % at 72h, which was lower than previously observed for these nanoparticles without the hydrogel.

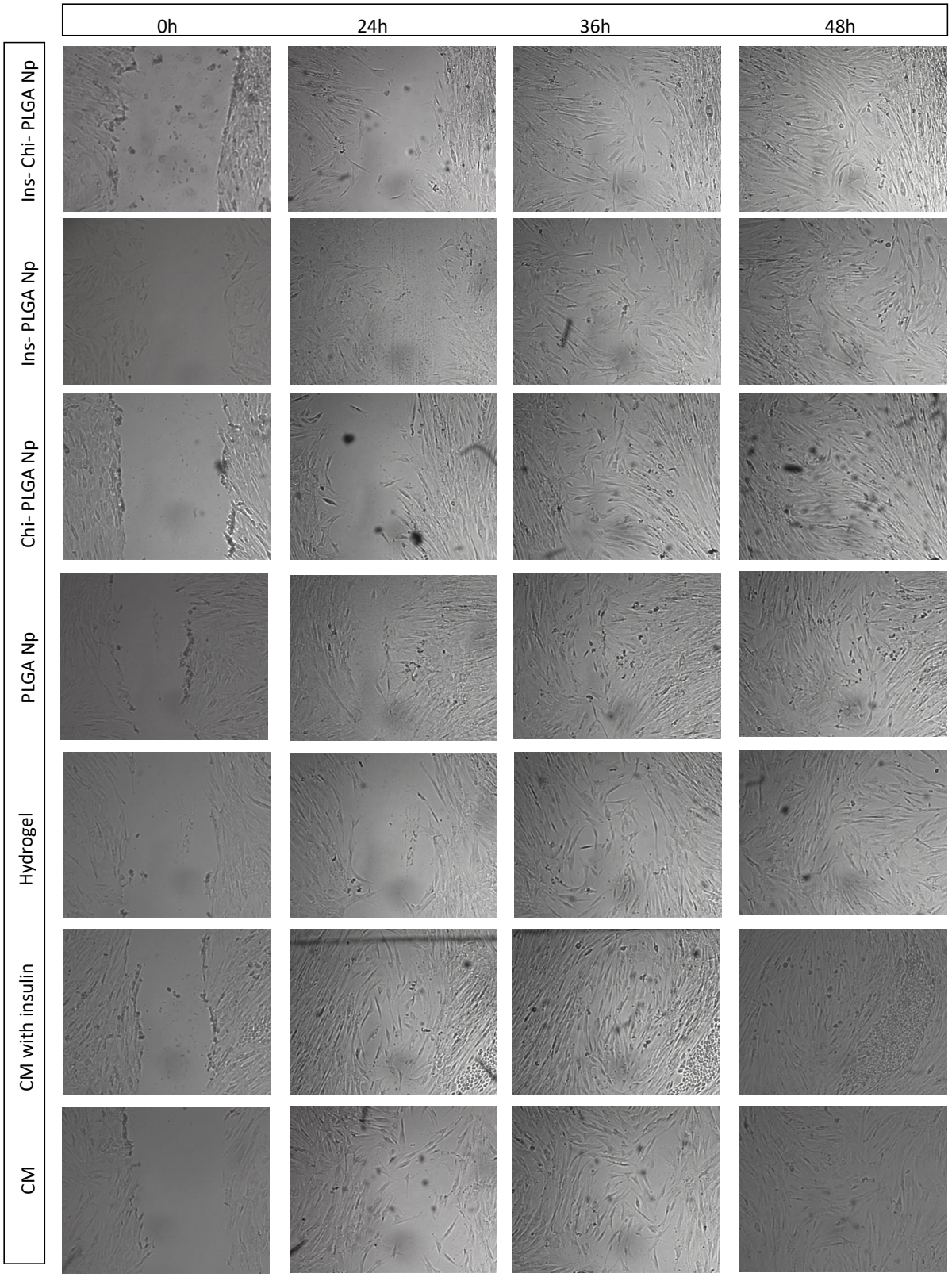

Figure 4.25: MSC cell scratch repair assays from Ins-Chi-Np-H, Ins-Np-H, Chi-Np-H, Np-H, Hydrogel, MSC expansion culture medium supplemented with insulin 10^{-7} M and MSC expansion culture medium. CM stands for culture medium.

4.3.3 Cytotoxicity assay

To assess the biocompatibility of the developed delivery system, a citotoxicity assay was performed. The cell viability % for each condition and concentration, 1:2 and 1:20, are shown in Table 4.6.

Table 4.6: L929 cell viability % at different concentrations, 1:2 and 1:20 and at different conditions: Ins-Chi-Np-H, Ins-Np-H, Chi-Np-H, Np-H, hydrogel, L929 expansion culture medium supplemented with insulin 10-7 M, expansion culture medium supplemented with 10% (v/v) DMSO (positive control) and L929 expansion culture medium (negative control). CM stands for culture medium.

Conditions	**Viability (%)**	
	1:2	1:20
Ins-Chi-Np-H	42	86
Ins-Np-H	43	80
Chi-Np-H	68	84
Np-H	53	78
Hydrogel	34	78
CM with insulin	97	
CM with DMSO (+control)	23	
CM (-control)	100	

The culture medium was used as a negative control, where 100% of the cells maintain their viability, and this value is used for comparison to other conditions. Cell viability reduced to less than 70% of the negative control is considered to have a cytotoxic potential. The culture medium with insulin showed great biocompatibility, which was expected. For the different hydrogels, in the concentration of 1:2, 5ml of culture + 5ml of hydrogel, all hydrogels showed cytotoxic potential. In contrary, for 1:20 concentration, all hydrogels showed biocompatibility. Cell viability was similar for the chitosan-coated nanoparticles, Ins-Chi-Np-H and Chi-Np-H with 86 and 84%, respectively, and similar for the other formulations, Ins-Np-H, Np-H and hydrogel with 80, 78 and 78%, respectively. The slight increase in cell viability for the formulations with chitosan, could be explained by the presence of the natural polymer, chitosan, which is known to have great biocompatibility owing to the similarity to macromolecules recognised by the human body.

Overall, with the right concentration, all the different hydrogels show good biocompatibility which is a great sign, for further use of this approach for *in vivo* testing.

Chapter 5

Conclusions

5.1 Achievements

This research aimed to develop a DDS to aid in chronic WH. In this work, PLGA nanoparticles with and without chitosan were produced with different compositions of chitosan. Later, the nanoparticles were embedded in a hydrogel, which also had different concentrations of alginate and glycerin, and a different number of freeze-thawing cycles. These variables were used to optimize the hydrogel-nanoparticles formulation to better suit topical application. Once the optimization was achieved, the optimal formulation was used for further tests with and without insulin loading. These tests aimed to test the bioactivity and structure of insulin after the encapsulation, and also to address the insulin release profile. After having a controlled release of bioactive insulin, *in vitro* tests followed to address the effectiveness of this approach on cell growth and migration.

With the use of a design-of-experiments approach, it was possible to understand the relationship between the variables given to the program - % of chitosan, alginate and glycerin, and number of freeze-thawing cycles - and the dependent variables - mean diameter, zeta potential, viscosity and spreadability. The variable with more significance was the amount of alginate, it was important for the change to negative zeta potential and the variance in the viscosity and spreadability, only in the mean diameter it did not have significance. With these correlations an optimal formulation for topical application was reached with a composition of 0.75% chitosan, 2% alginate, 6% glycerin and 1 freeze-thawing cycle at 20°C.

Continuing with the optimal formulation, the insulin was loaded in the nanoparticles and tests followed. The nanoparticles maintained their smooth surface and round shape after production and encapsulation of insulin, and after gelification. Results revealed that the insulin structure was preserved upon encapsulation and production of the hydrogel. The insulin release profile was also determined, and insulin was released in a sustained way, with results indicating that insulin probably continues to be released beyond the time studied. *In vitro* citotoxicity study revealed that all hydrogels showed biocompatibility. *In vitro* cell scratch assay showed enhanced cell migration for culture medium with insulin, but no enhanced cell migration was found in the hydrogel-nanoparticle systems when compared to the

controls.

Overall, all the proposed objectives for this thesis were achieved. Not only from the formulation point of view, to understand the relationship between each ingredient in the formulation and achieving the optimal formulation. But also, from the efficiency of this approach in protecting the insulin's bioactivity when encapsulated, the sustained release and the good biocompatibility of the delivery system. Only the efficiency of this approach in the promotion of *in vitro* cell migration for the developed systems was not as expected.

5.2 Future Work

It is important to point out the importance of continuing this research work whether to optimize the production of the DDS or to continue with *in vitro* or *in vivo* testing.

When it comes to the formulation point of view, future studies could test the relationship between the % of PVA in the formulation and the number of freeze thawing cycles and the effect it has in the viscosity of the formulation. This could be achieved by altering the concentration of PVA in the formulation as well as the number of freeze-thawing cycles, or even the temperature at which it is frozen, and studying the effects of the crooslinking reactions with water and PVA on the viscosity of the formulation.

The *in vitro* release assay should also be revised, since the methodology had some difficulties related to the little amount of receiver phase. Mainly, to obtain information of the total time it takes for 100% of the insulin to be released, it would be a good idea to extend the period of time of the assay. Having that information would be advantageous to fully understand the controlled and sustained release of insulin in this approach, and further investigate the frequency of dressing changes for *in vivo* testing.

For the *in vitro* cell scratch, based on the results, it should be considered a revision on the time at which measures of the empty area of the scratch are made. The reason for this is that at 48h all the gaps are closed, and from the beginning only tree time points are measured. Since the scratches rapidly closed, it would be beneficial to have more information on what happens between 0 and 24h, for example. Another suggestion would be to repeat the assay with the nanoparticles without the hydrogel, to understand the results obtained. The fact that none the insulin-loaded nanoparticles system had the ability of enhancing cell migration, could be explained with the repetition of this test but without the hydrogel. To comprehend if the hydrogel does act as a barrier for the insulin release, and therefore insulin-like effects could not be seen in cell migration, or if the insulin released lost its bioactivity and therefore insulin advantages were lost.

Finally, *in vitro* testing does not replace *in vivo* tests, since *in vitro* never truly acts like a living being, it only mimics parts of it. For this reason, further research in *in vivo* models is needed to fully comprehend the effectiveness of this approach.

References

[1] C. K. Sen, G. M. Gordillo, S. Roy, R. Kirsner, L. Lambert, T. K. Hunt, F. Gottrup, G. C. Gurtner, and M. T. Longaker. Human skin wounds: a major and snowballing threat to public health and the economy. *Wound Repair and Regeneration*, 17(6):763–771, 2009.

[2] A. J. Whittam, Z. N. Maan, D. Duscher, V. W. Wong, J. A. Barrera, M. Januszyk, and G. C. Gurtner. Challenges and opportunities in drug delivery for wound healing. *Advances in Wound Care*, 5(2): 79–88, 2016.

[3] N. B. Menke, K. R. Ward, T. M. Witten, D. G. Bonchev, and R. F. Diegelmann. Impaired wound healing. *Clinics in Dermatology*, 25(1):19–25, 2007.

[4] W. Wang, K.-j. Lu, C.-h. Yu, Q.-l. Huang, and Y.-Z. Du. Nano-drug delivery systems in wound treatment and skin regeneration. *Journal of Nanobiotechnology*, 17(1):82, 2019.

[5] G. Han and R. Ceilley. Chronic wound healing: a review of current management and treatments. *Advances in Therapy*, 34(3):599–610, 2017.

[6] I. Garcia-Orue, J. L. Pedraz, R. M. Hernandez, and M. Igartua. Nanotechnology-based delivery systems to release growth factors and other endogenous molecules for chronic wound healing. *Journal of Drug Delivery Science and Technology*, 42:2–17, 2017.

[7] V. Jayarama Reddy, S. Radhakrishnan, R. Ravichandran, S. Mukherjee, R. Balamurugan, S. Sundarrajan, and S. Ramakrishna. Nanofibrous structured biomimetic strategies for skin tissue regeneration. *Wound Repair and Regeneration*, 21(1):1–16, 2013.

[8] P. S. Korrapati, K. Karthikeyan, A. Satish, V. R. Krishnaswamy, J. R. Venugopal, and S. Ramakrishna. Recent advancements in nanotechnological strategies in selection, design and delivery of biomolecules for skin regeneration. *Materials Science and Engineering: C*, 67:747–765, 2016.

[9] S. Agarwal and K. Krishnamurthy. Histology, skin. *StatPearls*, 2019.

[10] M. Boer, E. Duchnik, R. Maleszka, and M. Marchlewicz. Structural and biophysical characteristics of human skin in maintaining proper epidermal barrier function. *Advances in Dermatology and Allergology/Postpy Dermatologii i Alergologii*, 33(1):1, 2016.

[11] J. G. BETTS, P. DESAIX, E. JOHNSON, J. E. JOHNSON, O. KOROL, D. KRUSE, B. POE, J. A. WISE, M. WOMBLE, and K. A. YOUNG. *Anatomy Physiology*. OpenStax, Houston, Texas, 2013.

[12] L. Eckhart, S. Lippens, E. Tschachler, and W. Declercq. Cell death by cornification. *Biochimica et Biophysica Acta (BBA)-Molecular Cell Research*, 1833(12):3471–3480, 2013.

[13] H. Yousef, M. Alhajj, and S. Sharma. Anatomy, skin (integument), epidermis. 2017.

[14] B. D. Hodge and R. T. Brodell. Anatomy, skin sweat glands. 2019.

[15] E. Hoover, S. Aslam, and K. Krishnamurthy. Physiology, sebaceous glands. *StatPearls*, 2020.

[16] A. Oryan and E. Alemzadeh. Effects of insulin on wound healing: a review of animal and human evidences. *Life Sciences*, 174:59–67, 2017.

[17] S. Bunman, N. Dumavibhat, W. Chatthanawaree, S. Intalapaporn, T. Thuwachaosuan, and C. Thongchuan. Burn wound healing: Pathophysiology and current managementof burn injury. *The Bangkok Medical Journal*, 13(2):91–91, 2017.

[18] C. Caramella, B. Conti, T. Modena, F. Ferrari, M. C. Bonferoni, I. Genta, S. Rossi, M. L. Torre, G. Sandri, M. Sorrenti, et al. Controlled delivery systems for tissue repair and regeneration. *Journal of Drug Delivery Science and Technology*, 32:206–228, 2016.

[19] T. Emanuelli, A. Burgeiro, and E. Carvalho. Effects of insulin on the skin: possible healing benefits for diabetic foot ulcers. *Archives of Dermatological Research*, 308(10):677–694, 2016.

[20] D. G. Greenhalgh. The role of growth factors in wound healing. *Journal of Trauma and Acute Care Surgery*, 41(1):159–167, 1996.

[21] A. Tellechea, E. Leal, A. Veves, and E. Carvalho. Inflammatory and angiogenic abnormalities in diabetic wound healing: role of neuropeptides and therapeutic perspectives. *The Open Circulation & Vascular Journal*, 3(1), 2010.

[22] A. Aicher, C. Heeschen, C. Mildner-Rihm, C. Urbich, C. Ihling, K. Technau-Ihling, A. M. Zeiher, and S. Dimmeler. Essential role of endothelial nitric oxide synthase for mobilization of stem and progenitor cells. *Nature Medicine*, 9(11):1370–1376, 2003.

[23] J. Moura, L. Da Silva, M. Cruz, and E. Carvalho. Molecular and cellular mechanisms of bone morphogenetic proteins and activins in the skin: potential benefits for wound healing. *Archives of Dermatological Research*, 305(7):557–569, 2013.

[24] D. Varsha. Skin ulcers and wounds – causes and care. URL `https://drvarsha.com/skin-ulcers-and-wounds-causes-and-care/`.

[25] S. M. Kulišić and J. Lipozenčić. Differential diagnosis of chronic leg ulcers. *Phlebolymphology*, 19 (4):204, 2012.

[26] T. A. Wilgus, S. Roy, and J. C. McDaniel. Neutrophils and wound repair: positive actions and negative reactions. *Advances in Wound Care*, 2(7):379–388, 2013.

[27] S. Khanna, S. Biswas, Y. Shang, E. Collard, A. Azad, C. Kauh, V. Bhasker, G. M. Gordillo, C. K. Sen, and S. Roy. Macrophage dysfunction impairs resolution of inflammation in the wounds of diabetic mice. *PloS One*, 5(3):e9539, 2010.

[28] W. Marhoffer, M. Stein, L. Schleinkofer, and K. Federlin. Evidence of ex vivo and in vitro impaired neutrophil oxidative burst and phagocytic capacity in type 1 diabetes mellitus. *Diabetes Research and Clinical Practice*, 19(3):183–188, 1993.

[29] S. N. Zykova, T. G. Jenssen, M. Berdal, R. Olsen, R. Myklebust, and R. Seljelid. Altered cytokine and nitric oxide secretion in vitro by macrophages from diabetic type ii-like db/db mice. *Diabetes*, 49(9):1451–1458, 2000.

[30] R. Gillitzer and M. Goebeler. Chemokines in cutaneous wound healing. *Journal of Leukocyte Biology*, 69(4):513–521, 2001.

[31] N. J. Turner and S. F. Badylak. The use of biologic scaffolds in the treatment of chronic nonhealing wounds. *Advances in Wound Ware*, 4(8):490–500, 2015.

[32] J. S. Boateng, K. H. Matthews, H. N. Stevens, and G. M. Eccleston. Wound healing dressings and drug delivery systems: a review. *Journal of Pharmaceutical Sciences*, 97(8):2892–2923, 2008.

[33] X. Li, Y. Liu, J. Zhang, R. You, J. Qu, and M. Li. Functionalized silk fibroin dressing with topical bioactive insulin release for accelerated chronic wound healing. *Materials Science and Engineering: C*, 72:394–404, 2017.

[34] H. Beele, F. Meuleneire, M. Nahuys, and S. L. Percival. A prospective randomised open label study to evaluate the potential of a new silver alginate/carboxymethylcellulose antimicrobial wound dressing to promote wound healing. *International Wound Journal*, 7(4):262–270, 2010.

[35] S. L. Percival, P. Bowler, and E. J. Woods. Assessing the effect of an antimicrobial wound dressing on biofilms. *Wound Repair and Regeneration*, 16(1):52–57, 2008.

[36] V. R. Krishnaswamy, M. Manikandan, A. K. Munirajan, D. Vijayaraghavan, and P. S. Korrapati. Expression and integrity of dermatopontin in chronic cutaneous wounds: a crucial factor in impaired wound healing. *Cell and Tissue Research*, 358(3):833–841, 2014.

[37] Y.-B. Kwon, H.-W. Kim, D.-H. Roh, S.-Y. Yoon, R.-M. Baek, J.-Y. Kim, H. Kweon, K.-G. Lee, Y.-H. Park, and J.-H. Lee. Topical application of epidermal growth factor accelerates wound healing by myofibroblast proliferation and collagen synthesis in rat. *Journal of Veterinary Science*, 7(2): 105–109, 2006.

[38] X.-J. Wang, G. Han, P. Owens, Y. Siddiqui, and A. G. Li. Role of tgfβ-mediated inflammation in cutaneous wound healing. In *Journal of Investigative Dermatology Symposium Proceedings*, volume 11, pages 112–117. Elsevier, 2006.

[39] R. H. Demling. The role of anabolic hormones for wound healing in catabolic states. *Journal of Burns and Wounds*, 4, 2005.

[40] J. M. Smiell, T. J. Wieman, D. L. Steed, B. H. Perry, A. R. Sampson, and B. H. Schwab. Efficacy and safety of becaplermin (recombinant human platelet-derived growth factor-bb) in patients with non-healing, lower extremity diabetic ulcers: a combined analysis of four randomized studies. *Wound Repair and Regeneration*, 7(5):335–346, 1999.

[41] G. R. Grotendorst, G. Martin, D. Pencev, J. Sodek, A. Harvey, et al. Stimulation of granulation tissue formation by platelet-derived growth factor in normal and diabetic rats. *The Journal of Clinical Investigation*, 76(6):2323–2329, 1985.

[42] F. Zhang, M. Lei, T. Oswald, Y. Pang, B. Blain, Z. Cai, and W. Lineaweaver. The effect of vascular endothelial growth factor on the healing of ischaemic skin wounds. *British Journal of Plastic Surgery*, 56(4):334–341, 2003.

[43] M. F. White. Insulin signaling in health and disease. *Science*, 302(5651):1710–1711, 2003.

[44] W. Landgraf and J. Sandow. Recombinant human insulins–clinical efficacy and safety in diabetes therapy. *European Endocrinology*, 12(1):12, 2016.

[45] H. Janßen, P. H. Janßen, and C. E. Broelsch. Uw is superior to celsior and htk in the protection of human liver endothelial cells against preservation injury. *Liver Transplantation*, 10(12):1514–1523, 2004.

[46] M. A. Christianson, M. W. Schwartz, and N. Suzuki. Determinants of insulin availability in parenteral nutrition solutions. *Journal of Parenteral and Enteral Nutrition*, 30(1):6–9, 2006.

[47] M. Hrynyk and R. J. Neufeld. Insulin and wound healing. *Burns*, 40(8):1433–1446, 2014.

[48] T. Satoh. Rho gtpases in insulin-stimulated glucose uptake. *Small GTPases*, 5(1):e28102, 2014.

[49] K. Siddle. Molecular basis of signaling specificity of insulin and igf receptors: neglected corners and recent advances. *Frontiers in Endocrinology*, 3:34, 2012.

[50] J. Zhang and F. Liu. Tissue-specific insulin signaling in the regulation of metabolism and aging. *IUBMB Life*, 66(7):485–495, 2014.

[51] C. V. Murphy, R. Coffey, C. H. Cook, A. T. Gerlach, and S. F. Miller. Early glycemic control in critically ill patients with burn injury. *Journal of Burn Care & Research*, 32(6):583–590, 2011.

[52] H. Brem, M. Tomic-Canic, et al. Cellular and molecular basis of wound healing in diabetes. *The Journal of Clinical Investigation*, 117(5):1219–1222, 2007.

[53] Y. Liu, M. Petreaca, and M. Martins-Green. Cell and molecular mechanisms of insulin-induced angiogenesis. *Journal of Cellular and Molecular Medicine*, 13(11-12):4492–4504, 2009.

[54] G. Tiwari, R. Tiwari, B. Sriwastawa, L. Bhati, S. Pandey, P. Pandey, and S. K. Bannerjee. Drug delivery systems: An updated review. *International Journal of Pharmaceutical Investigation*, 2(1): 2, 2012.

[55] A. S. Rathore. Follow-on protein products: scientific issues, developments and challenges. *Trends in Biotechnology*, 27(12):698–705, 2009.

[56] M. Hrynyk, M. Martins-Green, A. E. Barron, and R. J. Neufeld. Sustained prolonged topical delivery of bioactive human insulin for potential treatment of cutaneous wounds. *International Journal of Pharmaceutics*, 398(1-2):146–154, 2010.

[57] G. Gainza, S. Villullas, J. L. Pedraz, R. M. Hernandez, and M. Igartua. Advances in drug delivery systems (ddss) to release growth factors for wound healing and skin regeneration. *Nanomedicine: Nanotechnology, Biology and Medicine*, 11(6):1551–1573, 2015.

[58] M. Navarro and J. A. Planell. *Nanotechnology in regenerative medicine*. Humana Press, 2012.

[59] S. Deng, M. R. Gigliobianco, R. Censi, and P. Di Martino. Polymeric nanocapsules as nanotechnological alternative for drug delivery system: Current status, challenges and opportunities. *Nanomaterials*, 10(5):847, 2020.

[60] S. Sandhiya, S. A. Dkhar, and A. Surendiran. Emerging trends of nanomedicine–an overview. *Fundamental & Clinical Pharmacology*, 23(3):263–269, 2009.

[61] S. Parveen, R. Misra, and S. K. Sahoo. Nanoparticles: a boon to drug delivery, therapeutics, diagnostics and imaging. *Nanomedicine: Nanotechnology, Biology and Medicine*, 8(2):147–166, 2012.

[62] M. C. Ribeiro, V. L. R. Correa, F. K. L. da Silva, A. A. Casas, A. d. L. das Chagas, L. P. de Oliveira, M. P. Miguel, D. G. A. Diniz, A. C. Amaral, and L. B. de Menezes. Wound healing treatment using insulin within polymeric nanoparticles in the diabetes animal model. *European Journal of Pharmaceutical Sciences*, page 105330, 2020.

[63] K. K. Chereddy, R. Coco, P. B. Memvanga, B. Ucakar, A. des Rieux, G. Vandermeulen, and V. Préat. Combined effect of plga and curcumin on wound healing activity. *Journal of Controlled Release*, 171(2):208–215, 2013.

[64] Z. Değim. Use of microparticulate systems to accelerate skin wound healing. *Journal of Drug Targeting*, 16(6):437–448, 2008.

[65] H. Liu, C. Wang, C. Li, Y. Qin, Z. Wang, F. Yang, Z. Li, and J. Wang. A functional chitosan-based hydrogel as a wound dressing and drug delivery system in the treatment of wound healing. *RSC Advances*, 8(14):7533–7549, 2018.

[66] X. Lv, Y. Liu, S. Song, C. Tong, X. Shi, Y. Zhao, J. Zhang, and M. Hou. Influence of chitosan oligosaccharide on the gelling and wound healing properties of injectable hydrogels based on carboxymethyl chitosan/alginate polyelectrolyte complexes. *Carbohydrate Polymers*, 205:312–321, 2019.

[67] S. Maietta, R. De Santis, M. Catauro, M. Martorelli, and A. Gloria. Theoretical design of multilayer dental posts using cad-based approach and sol-gel chemistry. *Materials*, 11(5):738, 2018.

[68] S. Reitmaier, A. Shirazi-Adl, M. Bashkuev, H.-J. Wilke, A. Gloria, and H. Schmidt. In vitro and in silico investigations of disc nucleus replacement. *Journal of the Royal Society Interface*, 9(73): 1869–1879, 2012.

[69] G. Eke, N. Mangir, N. Hasirci, S. MacNeil, and V. Hasirci. Development of a uv crosslinked biodegradable hydrogel containing adipose derived stem cells to promote vascularization for skin wounds and tissue engineering. *Biomaterials*, 129:188–198, 2017.

[70] P. S. Patil, N. Fountas-Davis, H. Huang, M. M. Evancho-Chapman, J. A. Fulton, L. P. Shriver, and N. D. Leipzig. Fluorinated methacrylamide chitosan hydrogels enhance collagen synthesis in wound healing through increased oxygen availability. *Acta Biomaterialia*, 36:164–174, 2016.

[71] J. Wheeler, J. Woods, M. Cox, R. Cantrell, F. Watkins, and R. Edlich. Evolution of hydrogel polymers as contact lenses, surface coatings, dressings, and drug delivery systems. *Journal of Long-term Effects of Medical Implants*, 6(3-4):207–217, 1996.

[72] E. A. Kamoun, E.-R. S. Kenawy, and X. Chen. A review on polymeric hydrogel membranes for wound dressing applications: Pva-based hydrogel dressings. *Journal of Advanced Research*, 8(3): 217–233, 2017.

[73] T. D. Nguyen, T. T. Nguyen, K. L. Ly, A. H. Tran, T. T. N. Nguyen, M. T. Vo, H. M. Ho, N. T. N. Dang, V. T. Vo, D. H. Nguyen, et al. In vivo study of the antibacterial chitosan/polyvinyl alcohol loaded with silver nanoparticle hydrogel for wound healing applications. *International Journal of Polymer Science*, 2019, 2019.

[74] S. Dhall, J. P. Silva, Y. Liu, M. Hrynyk, M. Garcia, A. Chan, J. Lyubovitsky, R. J. Neufeld, and M. Martins-Green. Release of insulin from plga–alginate dressing stimulates regenerative healing of burn wounds in rats. *Clinical Science*, 129(12):1115–1129, 2015.

[75] B. A. Aderibigbe and B. Buyana. Alginate in wound dressings. *Pharmaceutics*, 10(2):42, 2018.

[76] G. Paradossi, F. Cavalieri, E. Chiessi, C. Spagnoli, and M. K. Cowman. Poly (vinyl alcohol) as versatile biomaterial for potential biomedical applications. *Journal of Materials Science: Materials in Medicine*, 14(8):687–691, 2003.

[77] A. Setia and P. Ahuja. Nanohydrogels: Emerging trend for drug delivery. In *Organic Materials as Smart Nanocarriers for Drug Delivery*, pages 293–368. Elsevier, 2018.

[78] Soap, D. Association, et al. Glycerine: an overview. *Terms, Technical Data, Properties, Performance*, 1990.

[79] P. Fonte, S. Soares, A. Costa, J. C. Andrade, V. Seabra, S. Reis, and B. Sarmento. Effect of cryoprotectants on the porosity and stability of insulin-loaded plga nanoparticles after freeze-drying. *Biomatter*, 2(4):329–339, 2012.

[80] M. T. Knorst. *Desenvolvimento tecnológico de forma farmacêutica plástica contendo extrato concentrado de Achyrocline satureioides (Lam.) DC. Compositae (marcela).* Master's thesis, Universidade Federal do Rio Grande do Sul, 1991.

[81] B. Sarmento, A. Ribeiro, F. Veiga, and D. Ferreira. Development and validation of a rapid reversed-phase hplc method for the determination of insulin from nanoparticulate systems. *Biomedical Chromatography*, 20(9):898–903, 2006.

[82] R. G. Loughlin, M. M. Tunney, R. F. Donnelly, D. J. Murphy, M. Jenkins, and P. A. McCarron. Modulation of gel formation and drug-release characteristics of lidocaine-loaded poly (vinyl alcohol)-tetraborate hydrogel systems using scavenger polyol sugars. *European Journal of Pharmaceutics and Biopharmaceutics*, 69(3):1135–1146, 2008.

[83] B.-S. Kim, C.-S. Kim, and K.-M. Lee. The intracellular uptake ability of chitosan-coated poly (d, l-lactideco-glycolide) nanoparticles. *Archives of Pharmacal Research*, 31(8):1050, 2008.

[84] M. do Céu Teixeira, A. Santini, and E. B. Souto. Delivery of antimicrobials by chitosan-composed therapeutic nanostructures. In *Nanostructures for Antimicrobial Therapy*, pages 203–222. Elsevier, 2017.

[85] M. Danaei, M. Dehghankhold, S. Ataei, F. Hasanzadeh Davarani, R. Javanmard, A. Dokhani, S. Khorasani, and M. Mozafari. Impact of particle size and polydispersity index on the clinical applications of lipidic nanocarrier systems. *Pharmaceutics*, 10(2):57, 2018.

[86] C. Su, Y. Feng, J. Ye, Y. Zhang, Z. Gao, M. Zhao, N. Yang, K. Nishinari, and Y. Fang. Effect of sodium alginate on the stability of natural soybean oil body emulsions. *RSC Advances*, 8(9):4731–4741, 2018.

[87] L. Buhse, R. Kolinski, B. Westenberger, A. Wokovich, J. Spencer, C. W. Chen, S. Turujman, M. Gautam-Basak, G. J. Kang, A. Kibbe, et al. Topical drug classification. *International Journal of Pharmaceutics*, 295(1-2):101–112, 2005.

[88] P. K. Bolla, B. A. Clark, A. Juluri, H. S. Cheruvu, and J. Renukuntla. Evaluation of formulation parameters on permeation of ibuprofen from topical formulations using strat-m® membrane. *Pharmaceutics*, 12(2):151, 2020.

[89] R. W. Frick. Accepting the null hypothesis. *Memory & Cognition*, 23(1):132–138, 1995.

[90] J. Frost. Understanding analysis of variance (anova) and the f-test. *The Minitab Blog. Pridobljeno*, 10(01):2017, 2016.

[91] L. L. dos Santos. Natural polymeric biomaterials: Processing and properties. In *Reference Module in Materials Science and Materials Engineering*. Elsevier, 2017.

[92] P. Fonte, F. Andrade, C. Azevedo, J. Pinto, V. Seabra, M. van de Weert, S. Reis, and B. Sarmento. Effect of the freezing step in the stability and bioactivity of protein-loaded plga nanoparticles upon lyophilization. *Pharmaceutical Research*, 33(11):2777–2793, 2016.

[93] H. LeVine. Thioflavine t interaction with amyloid β-sheet structures. *Amyloid*, 2(1):1–6, 1995.

[94] S. M. Kelly, T. J. Jess, and N. C. Price. How to study proteins by circular dichroism. *Biochimica et Biophysica Acta (BBA)-Proteins and Proteomics*, 1751(2):119–139, 2005.

[95] Z. Yong, D. Yingjie, W. Xueli, X. Jinghua, and L. Zhengqiang. Conformational and bioactivity analysis of insulin: Freeze-drying tba/water co-solvent system in the presence of surfactant and sugar. *International Journal of Pharmaceutics*, 371(1-2):71–81, 2009.

[96] M. Bouchard, J. Zurdo, E. J. Nettleton, C. M. Dobson, and C. V. Robinson. Formation of insulin amyloid fibrils followed by ftir simultaneously with cd and electron microscopy. *Protein Science*, 9 (10):1960–1967, 2000.

[97] I. B. Bekard and D. E. Dunstan. Tyrosine autofluorescence as a measure of bovine insulin fibrillation. *Biophysical Journal*, 97(9):2521–2531, 2009.

[98] M. Correia, M. T. Neves-Petersen, P. B. Jeppesen, S. Gregersen, and S. B. Petersen. Uv-light exposure of insulin: pharmaceutical implications upon covalent insulin dityrosine dimerization and disulphide bond photolysis. *PLoS One*, 7(12):e50733, 2012.

[99] J. R. Lakowicz. *Principles of fluorescence spectroscopy*. Springer, Boston, MA, 3 edition, 2006.